energies

MDPI

Review

Modeling, Design, and Optimization of Loop Heat Pipes

Yihang Zhao [1], Mingshan Wei [1,2,*] and Dan Dan [1]

[1] School of Mechanical Engineering, Beijing Institute of Technology, Beijing 100081, China; zhaoyihang1999@bit.edu.cn (Y.Z.); dandan@bit.edu.cn (D.D.)
[2] School of Mechanical and Electrical Engineering, China University of Mining and Technology-Beijing, Beijing 100083, China
* Correspondence: mswei@bit.edu.cn

Abstract: Thermal management technology based on loop heat pipes (LHPs) has broad application prospects in heat transfer control for aerospace and new energy vehicles. LHPs offer excellent heat transfer performance, reliability, and flexibility, making them suitable for high-heat flux density, high-power heat dissipation, and complex thermal management scenarios. However, due to limitations in heat source temperature and heat transfer power range, LHP-based thermal management systems still face challenges, especially in thermohydraulic modeling, component design, and optimization. Steady-state models improve computational efficiency and accuracy, while transient models capture dynamic behavior under various conditions, aiding performance evaluation during start-up and non-steady-state scenarios. Designs for single/multi-evaporators, compensation chambers, and wick materials are also reviewed. Single-evaporator designs offer compact and efficient start-up, while multi-evaporator designs handle complex thermal environments with multiple heat sources. Innovations in wick materials, such as porous metals, composites, and 3D printing, enhance capillary driving force and heat transfer performance. A comprehensive summary of working fluid selection criteria is conducted, and the effects of selecting organic, inorganic, and nanofluid working fluids on the performance of LHPs are evaluated. The selection process should consider thermodynamic properties, safety, and environmental friendliness to ensure optimal performance. Additionally, the mechanism and optimization methods of the start-up behavior, temperature oscillation, and non-condensable gas on the operating characteristics of LHPs were summarized. Optimizing vapor/liquid distribution, heat load, and sink temperature enhances start-up efficiency and minimizes temperature overshoot. Improved capillary structures and working fluids reduce temperature oscillations. Addressing non-condensable gases with materials like titanium and thermoelectric coolers ensures long-term stability and reliability. This review comprehensively discusses the development trends and prospects of LHP technology, aiming to guide the design and optimization of LHP.

Keywords: loop heat pipe; thermohydraulic modeling; component design; working fluids; operating characteristics

Citation: Zhao, Y.; Wei, M.; Dan, D. Modeling, Design, and Optimization of Loop Heat Pipes. *Energies* **2024**, *17*, 3971. https://doi.org/10.3390/en17163971

Academic Editors: Marco Lorenzini and Andrey A. Kurkin

Received: 8 July 2024
Revised: 27 July 2024
Accepted: 7 August 2024
Published: 10 August 2024

1. Introduction

Nowadays, the rapid development of aerospace technology, high-power electronics, data centers, and new energy vehicles has urgently increased the demand for thermal management [1,2]. Thermal components in these fields, such as spacecraft thermal control systems, chips, power batteries, and electric drives, have experienced notable increases in heat flux density [3–5]. Consequently, finding efficient thermal management solutions is crucial [6–8]. Loop heat pipes (LHPs), known for their excellent heat transfer efficiency and reliability, have emerged as promising candidates for managing high temperatures, high-heat flux densities, and high-power dissipation scenarios, attracting considerable research and attention [9,10].

LHPs are passive two-phase heat transfer devices that operate through a closed two-phase fluid circulation system maintained by a wick within the evaporator [11]. Derived

from traditional heat pipes, LHPs comprise an evaporator, compensation chamber (CC), condenser, vapor line, and liquid line. Smooth pipes connect the evaporator and condenser. At the same time, the adjacent compensation chamber facilitates liquid exchange. The working principle of LHPs is similar to that of traditional heat pipes. However, their capillary structure is confined to the evaporator, significantly reducing pressure drop within the wick and enhancing heat transfer efficiency [2]. The working fluid evaporates at the wick's outer surface when a heat load is applied to the evaporator. The resulting vapor flows through the vapor line to the condenser, condensing back into liquid and returning to the evaporator. This process is driven by capillary force and requires no external power [12]. LHPs overcome the inherent limitations of high flow resistance and sensitivity to gravity in traditional heat pipes. Their separate vapor and liquid channels prevent entrainment, improving heat transfer distance and anti-gravity capability [13]. With these advantages, LHPs demonstrate significant potential in thermal management applications.

Research on LHPs covers thermohydraulic modeling, component design, and operational characteristics. Current modeling includes steady-state and transient models, which capture LHP behavior under various conditions. Steady-state models simplify complex processes to explore key parameters affecting LHP performance [14]. Transient models address dynamic behavior, such as dry-out and bubble formation during startup. These models simulate instantaneous temperature and pressure distribution changes to evaluate system responses under non-steady-state conditions [15]. Most theoretical research focuses on steady-state performance. However, less attention is given to dynamic characteristics, and many assumptions limit these models' completeness [16].

Optimizing the structure and material selection of the evaporator, wick, and compensation chamber is crucial for enhancing LHP thermal performance. The configuration of the evaporators significantly impacts startup performance and heat transfer efficiency [17]. Porous metals, composite materials, and 3D-printed wicks can improve capillary driving force and heat transfer capabilities [18,19]. Additionally, the choice of working fluids is a key factor in LHP efficiency and stability. Thorough investigations of organic, inorganic, and nanofluids are necessary to determine their thermal properties and effectiveness in LHP applications. This research aims to find the optimal fluid combination for system performance enhancement [20]. For example, gravity-assisted heat pipes using acetone developed by Mousa et al. [21,22] demonstrated significant performance improvements in solar still applications. Due to their high thermal conductivity and excellent heat transfer properties, nanofluids are the current focus of research. Adding nanoparticles to traditional fluids can significantly improve LHP heat transfer efficiency [23]. Exploring these new materials and innovative designs is essential for further enhancing LHP performance in complex thermal management applications.

Research on optimizing the operational characteristics of LHPs is crucial for enhancing their heat transfer performance, operational adaptability, and stability. Current research focuses on startup behavior, temperature oscillations, and non-condensable gases (NCGs) [24]. Optimizing the startup process can improve the speed and reliability of heat transfer, allowing for rapid response in various environments [25]. Temperature oscillations during operation can affect system stability and efficiency. The research uses experiments and numerical simulations to analyze oscillation frequency and amplitude changes, exploring methods to control these oscillations [26]. Additionally, NCGs pose challenges during startup and operation by occupying space in heat transfer channels, increasing thermal resistance, and reducing efficiency. They also cause pressure fluctuations, complicating stable operation [27]. Therefore, analyzing LHP's operational characteristics and exploring optimization strategies is essential.

In summary, this paper comprehensively studies and analyzes key LHP technologies. The main content of this paper is outlined in Figure 1. Section 2 discusses the thermohydraulic modeling of LHPs, covering both steady-state and transient models and their application in optimizing LHP performance. Section 3 reviews the component design of LHPs, focusing on optimizing the evaporator, wick structure, and compensation chamber,

and evaluating their impact on overall thermal performance. Section 4 assesses the selection of various working fluids, including organic, inorganic, and nanofluids, analyzing their thermal properties and effectiveness in LHP applications. Section 5 explores the operational characteristics of LHPs, emphasizing startup behavior, temperature oscillation, and the effects of NCGs on LHP operation. This review provides theoretical support and design guidance for developing LHP technology.

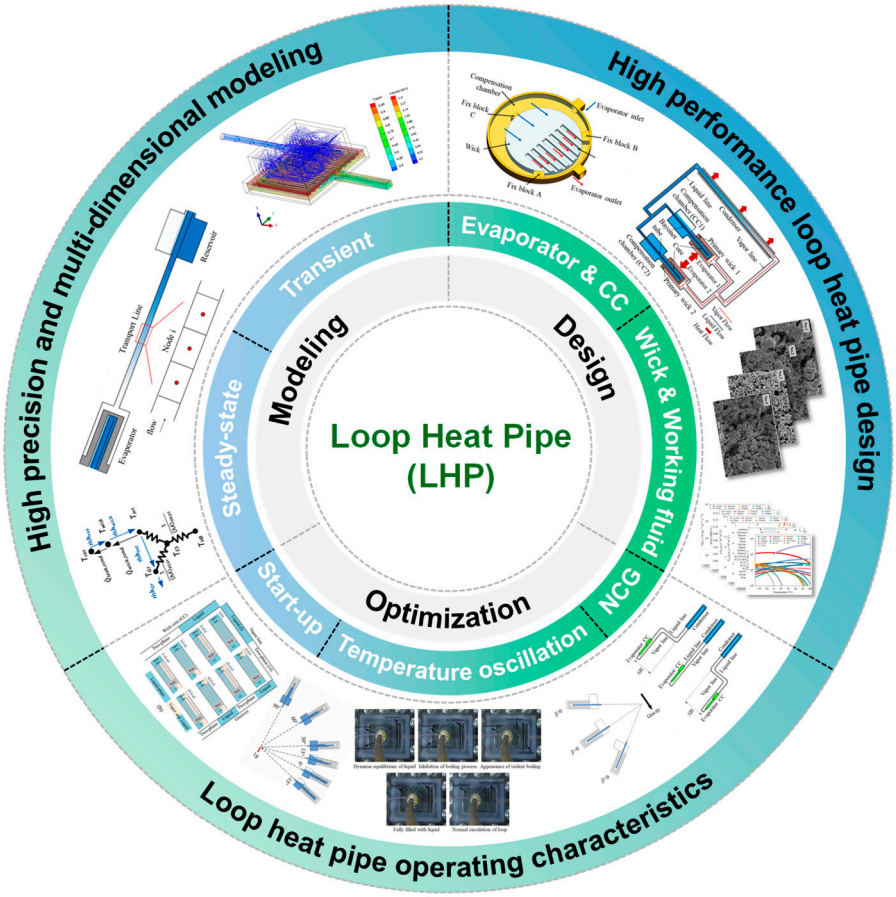

Figure 1. The main content of this paper.

2. Loop Heat Pipe Thermohydraulic Modeling

Precise modeling of LHPs' thermohydraulic behavior enables a comprehensive analysis of their performance and stability under various operational conditions. Such modeling facilitates design optimization and enhances heat transfer efficiency. Current research involves multidimensional steady-state and transient modeling to investigate the behavior of LHPs under stable and dynamic conditions, respectively. Steady-state models simplify the system to analyze key parameters and optimize performance under constant conditions. In contrast, transient models capture the system's response to changing conditions, including startup, shutdown, and varying heat loads. The thermohydraulic modeling overview of LHPs is shown in Figure 2.

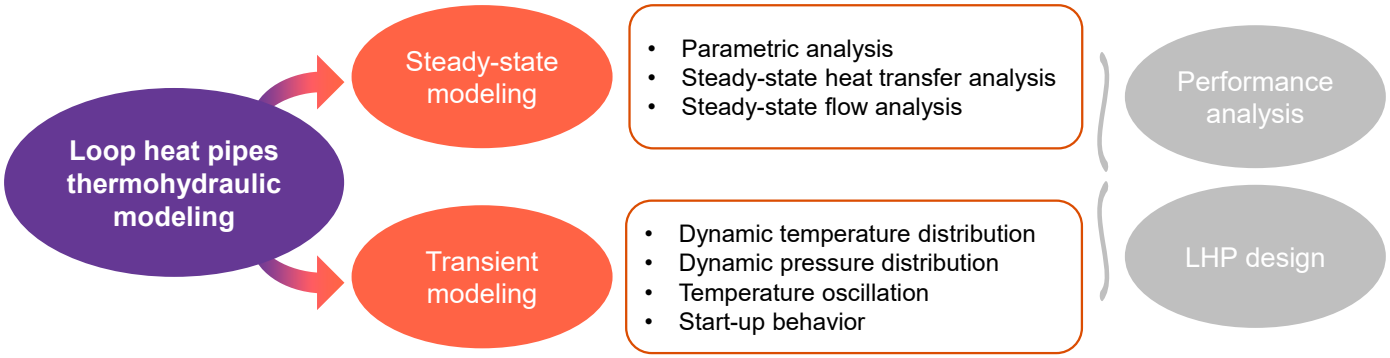

Figure 2. LHP thermohydraulic modeling overview.

2.1. Steady-State Modeling

Steady-state models of LHPs simplify complex physical processes, thereby improving computational efficiency. These models can analyze key parameters affecting LHP performance. Dickey and Peterson [28] proposed a model demonstrating the superior heat transfer capability of LHPs compared to conventional heat pipes. They also discussed steady-state temperature variations under different input power and adverse inclination angles. This model was further refined by incorporating steady-state energy conservation equations and pressure drop calculations along the fluid path, also considering heat exchange between various LHP components and the surrounding environment [29,30]. Experimental validations showed excellent agreement with theoretical predictions. Further, Hamdan et al. [31] described the steady-state thermodynamics, heat transfer, and fluid dynamics within LHPs based on conservation equations, thermodynamic relationships, and capillary and nucleate boiling limits. This research provides theoretical guidance for the detailed modeling and design of the wick in the evaporator of LHPs to improve the accuracy of the steady-state model.

A closed-form solution for LHP modeling that links operating temperature with various fluid and geometric parameters was proposed by Launay et al. [16]. This research ignored temperature variations in the vapor line and evaporator groove. Gabsi et al. [32] refined this model by introducing a heat transfer correlation for calculating evaporator thermal resistance and developing an analytical steady-state model based on momentum, energy conservation equations, and thermodynamic relationships. This model considers axial heat flux rates along the porous wick, through the evaporator wall, and heat dissipation via evaporation at the wick groove interface. Bai et al. [33] further refined the modeling of single-layer and double-layer composite wicks, as shown in Figure 3a. The model applied an annular flow model in the condenser, including the effects of liquid surface tension and liquid–vapor interaction. The derivation of the evaporator core's radial thermal conductivity assumes of one-dimensional heat transfer and flow. Additionally, the model assumes that the fluid within the condenser is homogeneous. They also developed a model for the steady-state operation of an LHP with a novel evaporator, which reduced heat leakage from the evaporator to the compensation chamber by actively adjusting the working fluid's phase distribution and flow path [34]. Furthermore, Bai et al. [35] also proposed a model for LHPs under gravity-assisted conditions, validated with experimental results and predicted operating characteristics. Jazebizadeh et al. [36] proposed a modular approach for constructing a steady-state LHP model, as depicted in Figure 3b, allowing easy extension to transient models. Qu et al. [37] developed a steady-state heat transfer model for an asymmetrical dual-evaporator LHP (DE-LHP), as presented in Figure 3c, modifying the mass flow distribution at the liquid line junction and proposing an influence range formula to determine position-dominant regions. The model assumes one-dimensional radial heat leakage along the capillary wick, considers the compensator and evaporator core in a vapor–liquid two-phase state, and neglects heat exchange between the vapor line and the environment. Meng et al. [38] formulated a one-dimensional steady-state mathematical

model for a novel LHP, which was validated through experimental data and included a parametric analysis of capillary wick material, diameter, length, and porosity. Du et al. [39] established a steady-state model for a novel plate LHP without a compensation chamber, achieving a maximum relative error of less than 15%. The model is simplified by assuming one-dimensional, incompressible flows of liquid and vapor, uniform fluid distribution within the LHP, and negligible pressure drop effects on vapor thermophysical properties during condensation. Additionally, it accounts for temperature-dependent changes in fluid properties while neglecting energy loss through the vapor line and vapor overheating in the evaporator, vapor line, and condenser. In a recent study, Li et al. [40] introduced a new numerical model to analyze the steady-state operating characteristics of flat plate LHPs under gravity-assisted conditions. Subsequently, Xia et al. [41] proposed an energy-coupled iterative thermal equilibrium calculation method, validating their models with experimental data to demonstrate the accurate simulation of LHP steady-state operation characteristics.

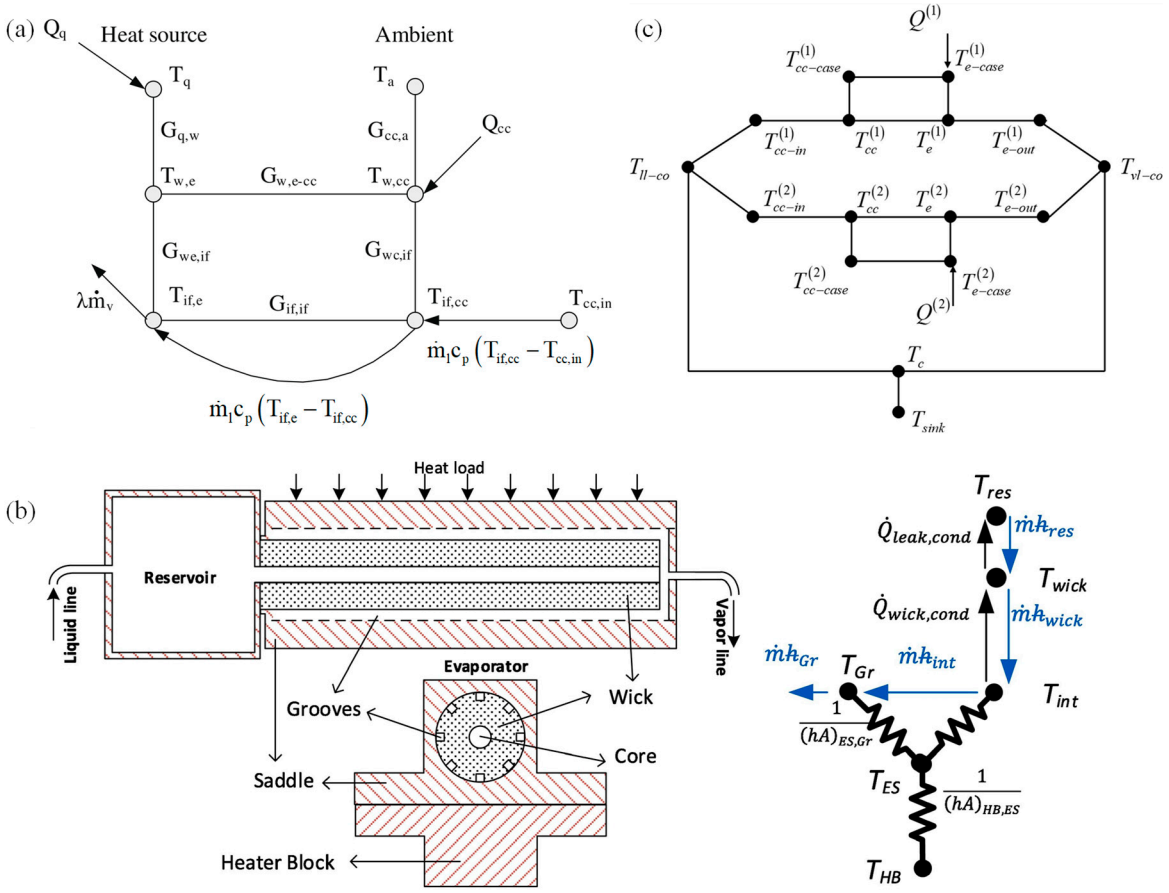

Figure 3. Thermal network diagrams in different models. (**a**) Evaporator and compensation chamber thermal network diagram [33]; (**b**) Evaporator diagram and node network [36]; (**c**) DE-LHP thermal network [37].

In addition to the zero-dimensional and one-dimensional models, Li et al. [42] developed a quasi-three-dimensional steady-state numerical model to investigate heat and mass transfer within square flat-plate evaporators featuring fully saturated wicking structures, as depicted in Figure 4a. The model employs an optimized mesh of 84,000 cells designed to improve boundary condition resolution and temperature accuracy at critical interfaces. This approach focuses on the wetted region, integrating conductive heat transfer with comprehensive mass transfer dynamics in the wicking structure, and incorporates phase change at the liquid–vapor interface. Zhang et al. [43] also established a detailed three-dimensional model to explore flow and heat transfer phenomena in micro LHP flat-plate evaporators,

considering the interplay between the sintered framework, vapor grooves, and wall conduction. Chernysheva and Maydanik [44,45] studied the three-dimensional case of heat and mass transfer in flat-plate copper–water LHP evaporators, addressing the heat transfer processes in the active zone, isolation layer, wall, and compensation chamber, as shown in Figure 4b. Additionally, Chernysheva et al. [46] presented a three-dimensional model focusing on the liquid fill within the compensation chamber, as shown in Figure 4c. The model employs a nonuniform mesh, with a higher density of cells in critical areas like the heating zone and vapor-removal grooves, to capture significant physical parameter gradients effectively. This model evaluates the working fluid's temperature distribution, streamlines, and velocity fields under varying heat loads, elucidating their effects on dry-out phenomena and evaporation front movement. Siedel et al. [47] proposed a two-dimensional analytical steady-state model by merging the energy balance equations of various LHP components to precisely simulate the temperature field within the evaporator, accounting for thermal contact resistance, wick thermal conductivity, and accommodation coefficient.

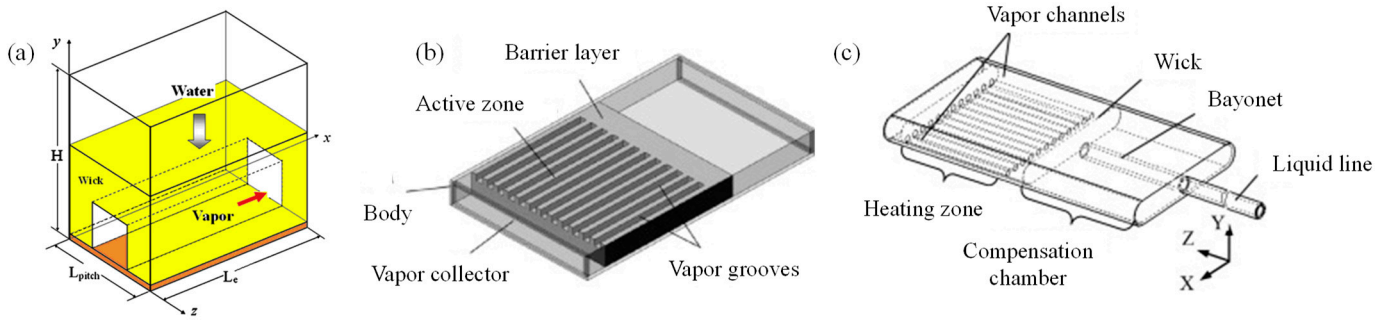

Figure 4. 3D evaporator computational domain. (**a**) Schematic of the computational model for the LHP evaporator [42]; (**b**) Configuration of flat evaporator model [44,45]; (**c**) Computer model of flat evaporator [46].

In summary, steady-state models of LHPs simplify complex physical processes and offer high computational efficiency. They enable the exploration of critical parameters affecting LHP performance, aiding design optimization. However, these models usually assume constant heat loads and stable conditions, potentially leading to inaccuracies in variable environments. Simplifying the complex interactions within LHP components can limit their applicability and accuracy. The dimensional assumptions in some models may also fail to accurately predict detailed temperature and pressure distributions.

2.2. Transient Modeling

Transient modeling captures the dynamic behavior of LHPs under various operating conditions, providing insights that can be used to improve their stability and reliability in complex scenarios. Murakoa et al. [48,49] developed a node-based mathematical model capable of simulating transient temperature and pressure distributions within an LHP. This zero-dimensional model can predict the formation of dry-out and bubbles during operation, offering critical insights into the stability and reliability of LHP systems. Launay et al. [50] advanced the field by dividing the LHP into subsystems and developing transient mass, energy, and momentum conservation equations for each subsystem. This approach effectively studied the oscillatory behavior during LHP operation and accurately predicted frequency and amplitude. Similarly, Adachi et al. [26,51] developed a transient model to investigate temperature oscillations in LHPs, focusing on steam parameters in the vapor line and examining the impact of heat load and sink temperature. Ren et al. [52] proposed an axisymmetric two-dimensional mathematical model to simulate heat transfer, flow, and evaporation within the capillary porous structure of cylindrical LHP evaporators. This model was validated by demonstrating the self-driven mechanism of "inverted meniscus" evaporators.

The temperature distribution in the compensation chamber was addressed by Shukla et al. [53] through a model solving the Fourier heat conduction equation in hollow cylinders. They also derived a one-dimensional transient model for vapor temperature in the condenser. The dynamic behavior of LHP units was successfully simulated using a modular approach by Kaya et al. [54]. This method allowed specific designs to be generated and applied to more complex designs with the EcosimPro software tool. A model that monitors the vapor–liquid interface in the condenser and liquid levels in the compensation chamber was developed by Vlassov et al. [55], which considered vapor phase entry and partial condensation. This model is essential for ensuring the efficiency and reliability of thermal regulation, particularly in systems where vapor phase dynamics are critical. Huang et al. [25] established a system dynamics model of LHPs to investigate start-up behavior, identifying four start-up modes based on heat load. This model can be used to optimize the startup characteristics of LHP in various situations. The system-level transient responses of LHP-microelectromechanical systems (MEMS) for thermal management were analyzed by Li et al. through hybrid models based on basic 3-node and 4-node thermal networks [56].

Additionally, Nishikawara et al. [55] proposed a one-dimensional transient mathematical model to predict the dynamic behavior of LHPs and address time lag issues between simulation and experimental results. Boubaker et al. [57] introduced a transient model for capillary pumped loops, accurately depicting phase change phenomena within the evaporator. Bernagozzi et al. [58] proposed a transient lumped parameter model for LHPs in electric vehicle energy management, validated through parameter analysis. Zhang et al. [59] used CFD simulations to analyze heat leakage in LHPs to optimize performance by improving materials and structures. He et al. [60] developed a transient model for a neon-charged low-temperature LHP, considering gravity effects and component layout orientations. Hashimoto et al. [61] noted that analyzing the transient phenomena of LHP requires extensive and complex computations. These calculations involve the coupling of heat transfer and fluid dynamics processes. Due to the complexity of transient phenomena and the need for high spatiotemporal resolution, traditional explicit methods require very small time steps and fine discretization, often taking several hours to complete. Consequently, their study employed an implicit solution method to reduce computation time, developing a multi-dimensional transient model for electric vehicle battery heating, as shown in Figure 5a. Hoang et al. [62] also emphasized the demand for a high-fidelity and efficient model to predict the transient behavior of LHPs and optimize LHP-based thermal management systems. Recently, Zhang et al. [63] developed a three-dimensional computational fluid dynamics (CFD) model to simulate heat and mass transfer in a flat evaporator, as shown in Figure 5b. The mesh quality of the model is ensured with a Cartesian hexahedral mesh for both solid and fluid domains, with a total of 1,393,776 elements and 1,237,562 nodes, optimized via a mesh independence study that confirmed the accuracy of results against experimental data. This model demonstrates high accuracy with an error of less than 10.29% when validated against experimental data.

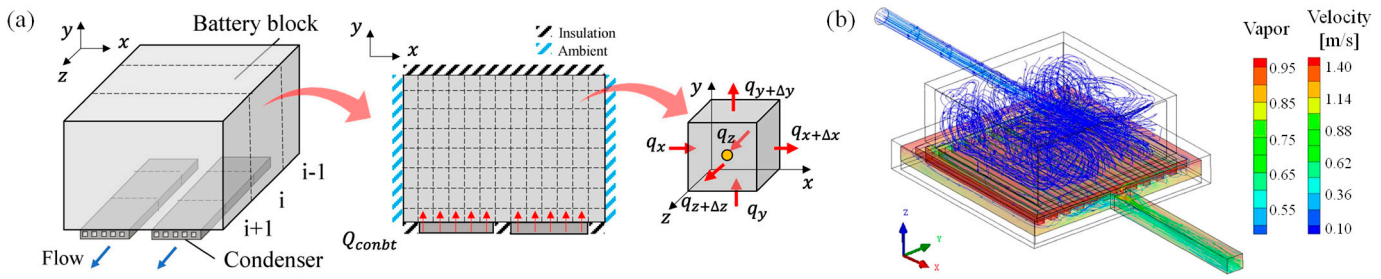

Figure 5. (**a**) Discrete cells of battery blocks and pipeline thermal network diagram based on node network method [61]; (**b**) Three-dimensional gas phase distribution and streamlined simulation of LHP evaporator [63].

In summary, transient models can capture the dynamic behavior of LHPs under various operating conditions. These models can simulate transient temperature and pressure variations, predicting critical phenomena such as dry-out and bubble formation during operation. Furthermore, by dividing the system into subsystems and establishing transient conservation equations, these models can effectively study oscillatory behavior and temperature oscillations, accurately predicting frequency and amplitude. However, transient models do face challenges, including complex computational requirements and the need for high-precision descriptions of physical phenomena. Despite these challenges, transient models remain an invaluable tool for optimizing the design of LHP.

3. Loop Heat Pipe Evaporator, Compensation Chamber, and Wick Design

The evaporator, compensation chamber, and wick are crucial components for receiving heat input and ensuring efficient operation in LHPs. The evaporator absorbs heat and directly affects the startup performance and heat transfer efficiency of the LHP. A well-designed evaporator ensures rapid vaporization of the working fluid, enhancing overall system performance. The compensation chamber is essential for the storage and stable supply of the working fluid. It maintains the liquid inventory and compensates for any volume changes due to temperature fluctuations or phase changes, ensuring continuous operation without interruptions. The wick, typically made of porous materials, generates the capillary force needed to circulate the working fluid throughout the LHP. This section focuses on the structural design of the evaporator and compensation chamber and the material innovations in wick design. The research overview of evaporator, wick, and condenser design is shown in Figure 6.

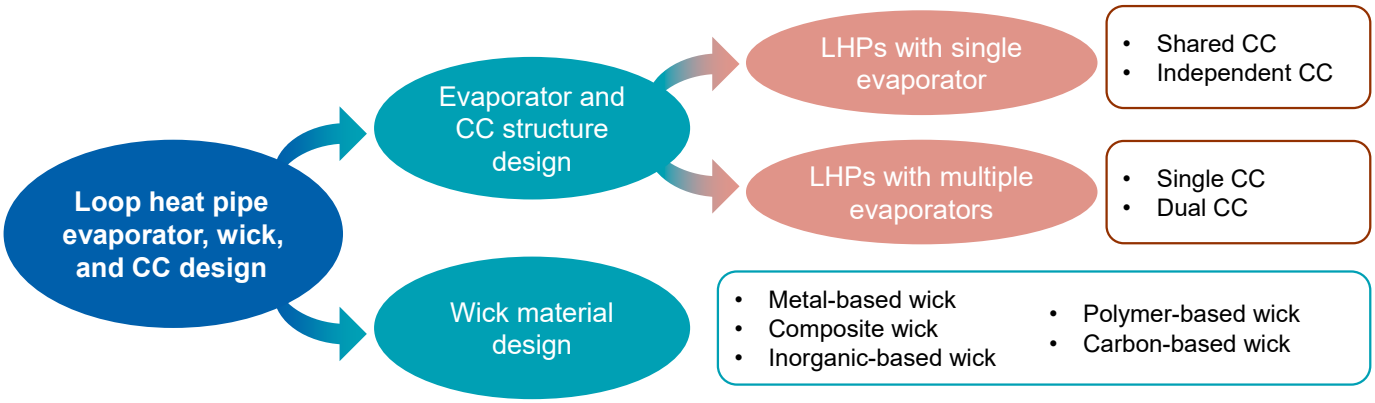

Figure 6. Overview of research on evaporator, compensation chamber, and wick design.

3.1. Evaporator and Compensation Chamber Structure Design

3.1.1. LHP with Single Evaporator

The thermal management capabilities of LHPs with single evaporators have been extensively studied to enhance their performance across various applications. One notable design by Li et al. [64] featured a compact copper–water LHP with a unique flat square evaporator, as shown in Figure 7a. This structure demonstrated the ability to achieve energy balance while transferring heat loads exceeding 600 W with a heat flux over 100 W/cm^2, indicating its suitability for high-performance cooling capabilities advantageous for electronic cooling applications. Furthermore, an innovative evaporator design was introduced by Song et al. [65], featuring a novel secondary wick structure made of 400-mesh stainless steel mesh, as depicted in Figure 7b. This secondary wick improved the seal between the evaporator and the working fluid flow path, enhancing start-up performance and heat load response speed. Additionally, it provided a liquid supply between the compensation chamber and the evaporator, increasing capillary action and reducing heat leakage.

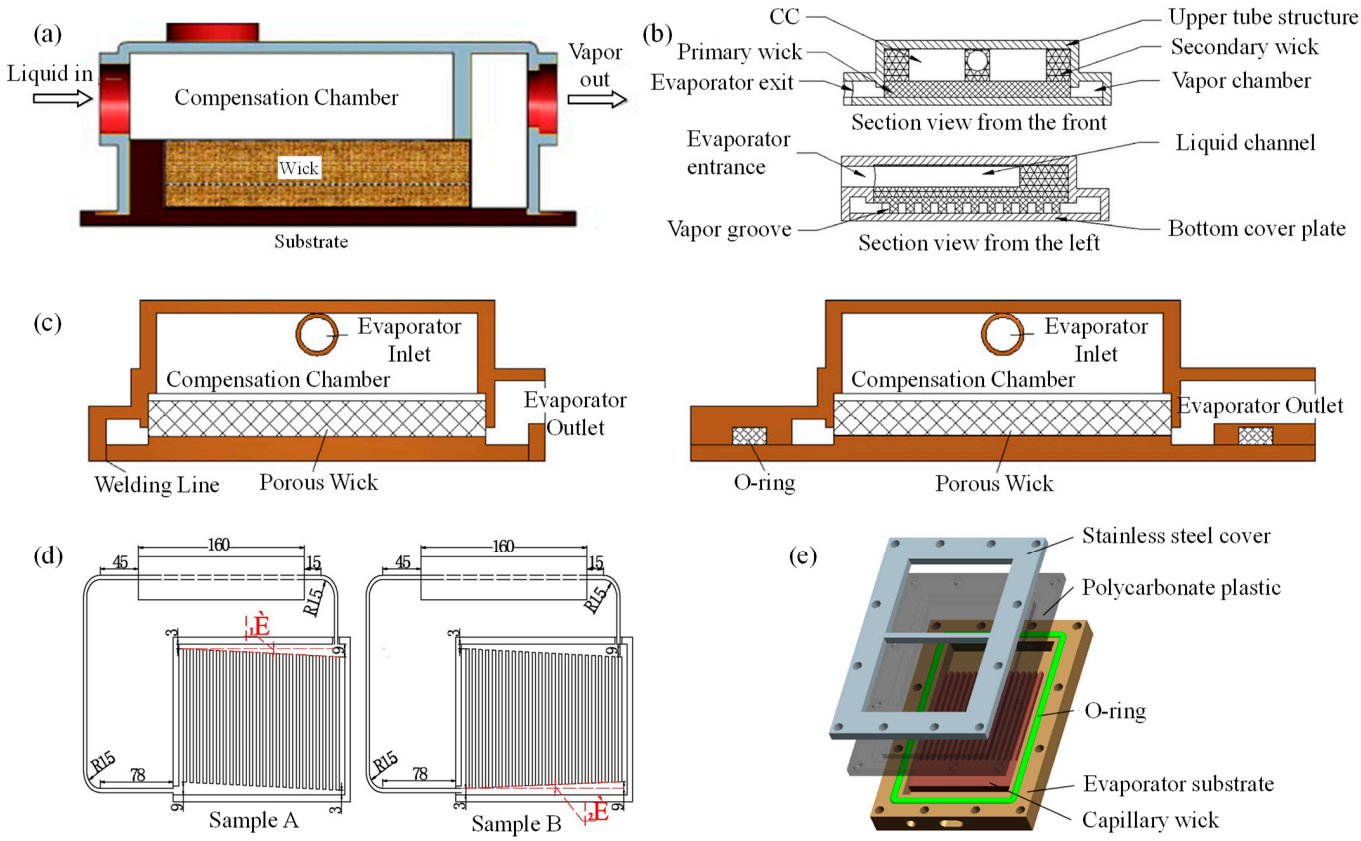

Figure 7. Structural diagrams of different LHP evaporators. (**a**) Inner structure of the LHP evaporator [64]; (**b**) Assembly diagram of the evaporator structure [65]; (**c**) Structure of the evaporator of the LHP [66]; (**d**) The schematic diagram of evaporator structure of ULHP [67]; (**e**) Configuration of the evaporator [68].

Wang et al. [66] explored the heat transfer characteristics of a miniature LHP with a disk-shaped evaporator, focusing on the influence of the sealing methods on LHP performance, as illustrated in Figure 7c. They found that brazed seals improved start-up performance and heat load operation by reducing heat leakage to the compensation chamber and increasing system vacuum, thus enhancing evaporative efficiency and overall thermal transfer capacity. This work builds upon the findings of Song et al. [65], which focused on sealing and fluid path optimization. In another study, Hong et al. [67] compared two ultra-thin LHPs (ULHP) with parallelogram and trapezoidal evaporator structures, as shown in Figure 7d. The findings indicated that the parallelogram configuration exhibited superior flow stability in various orientations, particularly at smaller inclination angles. This provides an alternative structural design to enhance LHP performance under specific conditions highlighted by previous studies. Investigating the two-phase flow characteristics of a compact copper–water LHP with a flat evaporator under gravity mode, Zhou et al. [68] demonstrated that the flat evaporator offered higher thermal conductivity and lower thermal resistance than traditional cylindrical evaporators. The energy balance can be achieved under a 500 W heat load, with a thermal resistance as low as 0.068 °C/W, as shown in Figure 7e.

A novel micro LHP (mLHP) with an eccentric evaporator was developed by Tian et al. [69], as illustrated in Figure 8a. This design permitted stable operation across a heat load range from 2 W to 60 W, with a minimum evaporator thermal resistance of 0.27 °C/W at a maximum heat load of 60 W and an overall system thermal resistance of approximately 1.3 °C/W. Their study also highlighted the effects of heat sink temperature on mLHP performance. Furthermore, Odagiri and Nagano [70] optimized the width and number of vapor grooves in a planar rectangular evaporator, enhancing heat transfer performance under

high-heat flux conditions. They designed an evaporator with 84 vapor grooves, each 0.3 mm wide, within a porous wick, as shown in Figure 8b. A comparative analysis of cylindrical and flat LHP evaporators was conducted by Maydanik et al. [71], discovering comparable thermal resistance and maximum heat flux. The cylindrical evaporator exhibited a marginal thermal performance advantage at non-horizontal angles, while the flat evaporator was more compact and lighter. Introducing an evaporator design for a dual compensation chamber LHP (DCCLHP), Wang et al. [72] created a configuration that allowed effective functioning even with adverse inclinations between the evaporator and the compensation chamber. This innovation expanded the potential for ground applications. A flat LHP (FLHP) evaporator with a reinforced structure was designed by Zhang et al. [73] and can withstand high working fluid pressures. This design is suitable for cooling equipment in space without additional brackets, thereby reducing thermal resistance. Li et al. [74] compared three LHP evaporator designs with varying configurations of vapor channels and wick contact. The results indicated that reducing the contact area between the wick and the heating surface improved LHP performance. The configuration with a separated wick and heating surface exhibited the lowest operating temperature and shortest start-up time. Xiong et al. [75] developed an LHP evaporator with dual-row vapor channels in a porous copper wick to enhance heat transfer performance. This configuration demonstrated superior thermal characteristics when handling high-heat flux server CPUs. Incorporating small copper powder particles and stainless-steel rings enhanced structural strength and improved liquid saturation, resulting in better operational thermal characteristics under high-heat flux conditions.

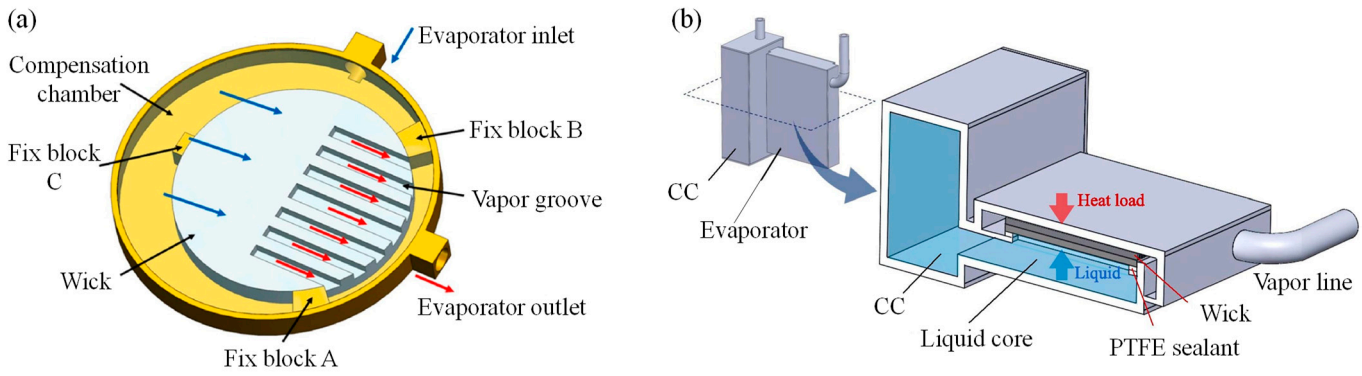

Figure 8. Different evaporators and compensation chamber structure diagrams. (**a**) Structure of the mLHP's evaporator [69]; (**b**) Evaporator structure [70].

3.1.2. LHP with Multiple Evaporators

The increasing integration of high-power electronic devices has created a critical need for efficient thermal management. High-heat flux and multiple heat sources present significant challenges, particularly in complex thermal environments. Multi-evaporator two-phase loop systems have demonstrated outstanding potential in such conditions, especially as thermal control systems transition to more integrated approaches [17]. Multi-evaporator LHPs are typically classified into two categories: those with multiple evaporators sharing a single compensation chamber and those with multiple evaporators, each with their own compensation chamber, as illustrated in Figure 9. The former configuration is often susceptible to instability during start-up and exhibits reduced heat transfer capability. In contrast, the latter maintains the advantages of traditional LHPs but may limit the number of evaporators.

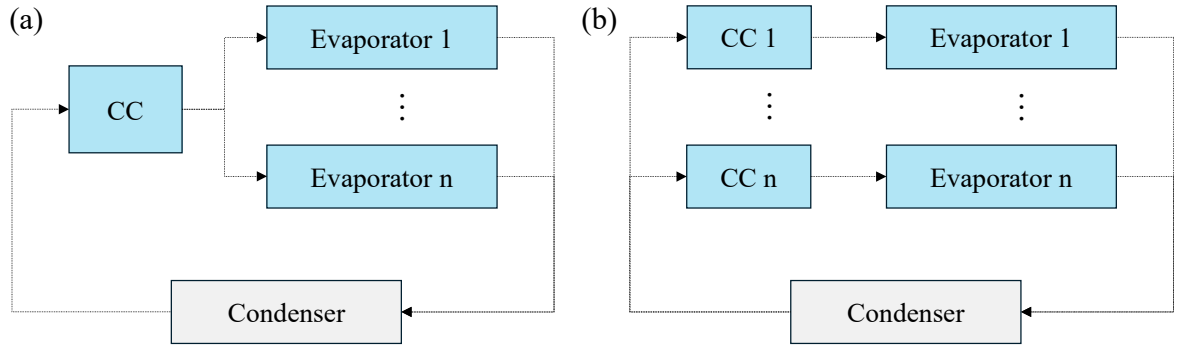

Figure 9. Two types of multi-evaporators LHP structures. (**a**) Multi-evaporator sharing standard compensation chamber; (**b**) Multi-evaporator each with its own compensation chamber.

Early studies conducted theoretical analysis and tests on dual-evaporator LHPs [76], focusing on regular operation and heat load-sharing modes. This foundational work provided critical insights into the behavior of multi-evaporator LHPs under varying thermal loads. Building on this, subsequent research introduced a multi-evaporator LHP (MLHP) [77,78], as shown in Figure 10a, which offers flexible thermal management by allowing simultaneous heating of two evaporators or selective heating in a heat load-sharing mode. Visual experiments under gravity-assisted conditions revealed the vapor–liquid distribution within the evaporator core and compensation chamber and the two-phase flow regions in the condenser, thereby demonstrating the practical applications of earlier theoretical findings. Further development led to a dual-evaporator LHP with an eccentric evaporator-compensation chamber configuration [79]. This innovative design maintains the evaporator and compensation chamber on the same horizontal plane in a gravitational field, reducing liquid backflow. Enhancements to the multi-evaporator design resulted in a dual-evaporator flat LHP with independent vapor transport lines for each evaporator [80], as illustrated in Figure 10b. This configuration includes interconnected compensation chambers and pipes, circumventing direct vapor interference between evaporators while effectively dissipating heat from two separate sources.

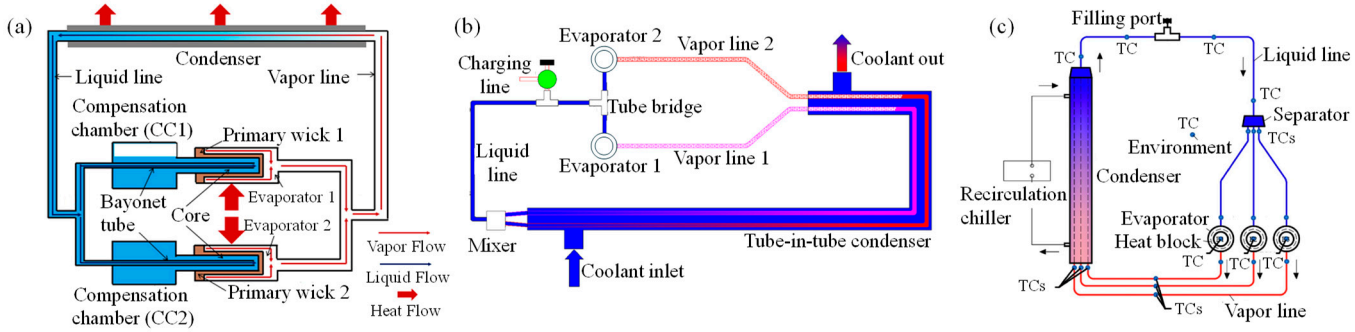

Figure 10. Different LHP structures with multi-evaporators. (**a**) Schematic of the MLHP with two evaporators [77]; (**b**) Diagram of the LHP with dual evaporators [80]; (**c**) System diagram of the flat disk ME-LHP [81].

Furthermore, Wu et al. [81] introduced an MLHP, as shown in Figure 10c, which is similar to He et al.'s [80] design but features three evaporators, each with an independent vapor line to reduce flow resistance and pressure drop losses. Wu's inclusion of a liquid separator to buffer the working fluid enhances fluid distribution flexibility, ensuring regular operation even if not all evaporators start simultaneously. Most recently, Lu et al. [82] also proposed an ME-LHP to reduce flow resistance differences among loops, thereby minimizing the likelihood of dry-out in the main loop (the loop with the highest flow resistance). This progression illustrates a clear trajectory from theoretical exploration to

practical, scalable solutions for complex thermal management challenges in high-power electronic systems.

In summary, the research on the structure design of LHP evaporator and compensation chamber shows the innovative design of single evaporator and multi-evaporator configurations. The single evaporator LHP provides better heat transfer and start-up performance through designs such as compact flat evaporators. The multi-evaporator LHP solves the challenges of high-heat flux and multi-heat sources and provides a flexible thermal management solution. This design minimizes flow resistance and improves stability. Future research should continue to optimize the design to enhance thermal performance further and improve the application potential of LHP in various applications.

3.2. Wick Material Design

3.2.1. Metal-Based Wick

The potential of metal-based wicks to enhance the thermal performance of LHPs is demonstrated through various material and structural optimizations. Giraudon et al. [83] showed that polishing or coating with thin gold layers could improve copper and zirconia wicks' manufacturing and surface characteristics. Polished copper wicks exhibited reduced thermal performance when gaps were smaller than the pore size due to increased thermal contact resistance. In contrast, gold-coated zirconia wicks benefited from reduced thermal contact resistance and enhanced surface wettability. Yeh et al. [84] achieved a remarkable evaporative heat transfer coefficient of up to 64,000 W/m^{2}K, approximately six times higher than single-pore wicks, by utilizing dual-pore structures that enhanced macropore connectivity and surface area for liquid film evaporation. Zhang et al. [85] demonstrated that dual-pore wicks combining large and small pores exhibited reduced flow resistance and maintained sufficient capillary force, as illustrated in Figure 11a. These wicks could handle a heat load of up to 330 W with a minimum thermal resistance of 0.161 °C/W. The multi-scale porous wicks developed by Ji et al. [86] demonstrated enhanced start-up times, as illustrated in Figure 11b. They also exhibited reduced wall temperatures and stabilized temperature fluctuations, achieving a maximum heat load of 110 W horizontally and 330 W when tilted, with thermal resistances of 0.382 °C/W and 0.161 °C/W, respectively.

Ling et al. [87,88] developed porous copper fiber sintered sheets (PCFSS) with composite porosities, as depicted in Figure 11c,d. Their findings indicated that these led to lower evaporator wall temperatures and thermal resistance. The LHP could handle up to 200 W and exhibited a thermal resistance of 0.047 °C/W. Hu et al. [89] demonstrated that 3D printing could be used to create stainless steel wicks with controlled structural parameters, as shown in Figure 11e, achieving a maximum heat transfer coefficient of 44,379 W/(m^2·K) and stable operation across various heat loads. This evidence illustrates the potential of 3D printing in advanced LHP wick fabrication. Zhang et al. [90] developed aluminum micro-groove wicks with reentrant cavity arrays using orthogonal extrusion, as illustrated in Figure 11f. Their findings indicated that increased extrusion spacing and depth improved permeability and capillary performance. Studies by Deng et al. [91] and Corrochano et al. [92] on nickel and stainless steel wicks revealed that stainless steel, with high porosity and permeability, ensured low heat leakage and high overall LHP performance due to its lower thermal conductivity. Esarte et al. [93] demonstrated that wicks manufactured using selective laser melting (SLM) exhibited excellent capillary action and permeability, outperforming traditional powder sintering and mesh technologies. The precise control of pore size and distribution afforded by SLM optimized LHP thermal performance, particularly in 80 W heat transfer applications.

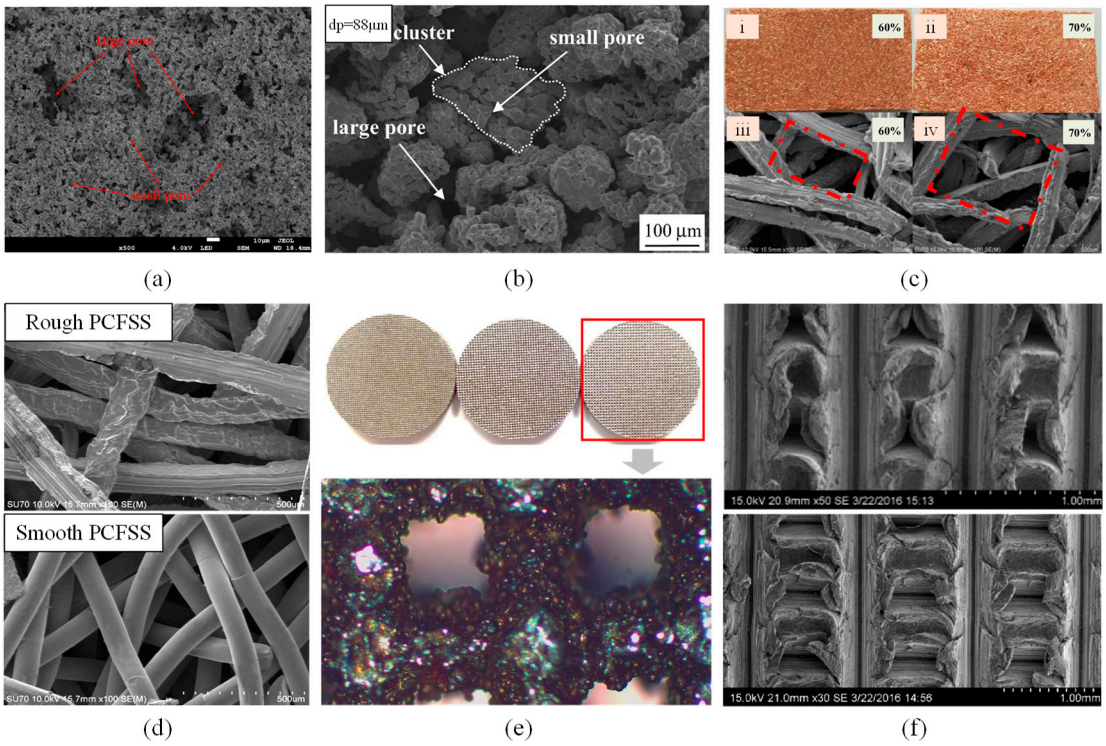

Figure 11. SEM images of metal-based wicks. (**a**) Biporous wick [85]; (**b**) Primary layer wick [86]; (**c**) Composite PCFSS wick: (**i**,**iii**) front side of 60% porosity; (**ii**,**iv**) reverse side of 70% porosity. (Dashed line box: pore size) [87]; (**d**) PCFSS wick [88]; (**e**) 3D-printed wick (Red box: sample C) [89]. (**f**) MGRA [90].

3.2.2. Polymer-Based Wick

Polymers such as polytetrafluoroethylene (PTFE) have emerged as viable materials for LHP wicks. Wu et al. [94] identified PTFE particles with a size range of 300 to 500 μm as the optimal choice. This particle size offers performance comparable to traditional metal wicks, with benefits including reduced costs and oxidation resistance. Wu et al. [95,96] enhanced the wettability of PTFE wicks by adding butanol to water, as presented in Figure 12. This resulted in achieving heat transfer capacities of up to 400 W, with a thermal resistance of 0.32 °C/W and a heat flux of 20 W/cm^2. Nishikawara et al. [97] optimized PTFE wicks for micro-LHPs, finding that a 20 μm gap between the wick and the shell provided the best heat transfer performance by maximizing the contact area for heat transfer and minimizing thermal resistance. Furthermore, a PTFE wick thickness of 2 mm minimized heat leakage, thereby improving system performance. The wicks could handle a heat load of up to 600 W with a thermal resistance of 0.249 °C/W. Overall, PTFE-based LHP wicks can reduce thermal resistance while maintaining high-heat transfer performance.

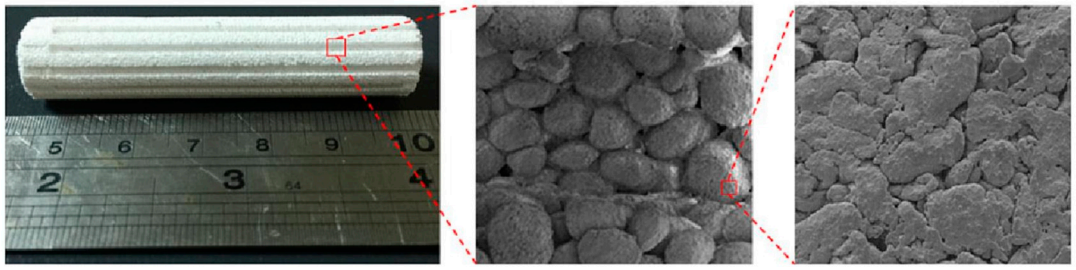

Figure 12. PTFE wick structure and SEM [95].

3.2.3. Composite and Inorganic-Based Wick

Hybrid and composite wicks combine different materials and structures to improve the performance of LHP further. These wicks demonstrated the potential for enhanced capillary action in two-phase heat transfer devices. He et al. [98] introduced a low-cost casting wick composed of cement and a blinder, with pore sizes ranging from 3 µm to 10 µm and porosity between 35% and 45%. This wick enables their LHP system to start horizontally within a 5 W to 80 W heat load range while maintaining evaporator surface temperatures below 100 °C. Xu et al. [99] combined high-permeability liquid transport layers with efficient evaporation layers in dual-layer composite copper wicks, reducing vapor traps and dry-out phenomena under high-heat loads. This design achieved a maximum heat load of 140 W, a heat transfer coefficient of 30,794 W/m^{2}K, and a thermal resistance of 0.046 °C/W, showcasing the advantages of combining diverse material properties to enhance LHP performance.

Wang et al. [100] proposed a composite wick structure comprising spherical and dendritic powders, as presented in Figure 13. Their findings show that the dual-pore structure effectively reduced the effective thermal conductivity and enhanced liquid transportation, which is crucial for high-heat flux applications. Yang et al. [101] developed a silicon nitride capillary wick with an eccentric structure for DCCLHP, showing that this design could reliably initiate under low-heat loads and effectively suppress back heat leakage, enhancing thermal performance. Zhou et al. [102] employed multi-layer metal foams. The results indicated that copper foam, with its higher thermal conductivity, exhibited superior performance to nickel foam, maintaining evaporator temperatures below 90 °C under a 30–100 W heat load.

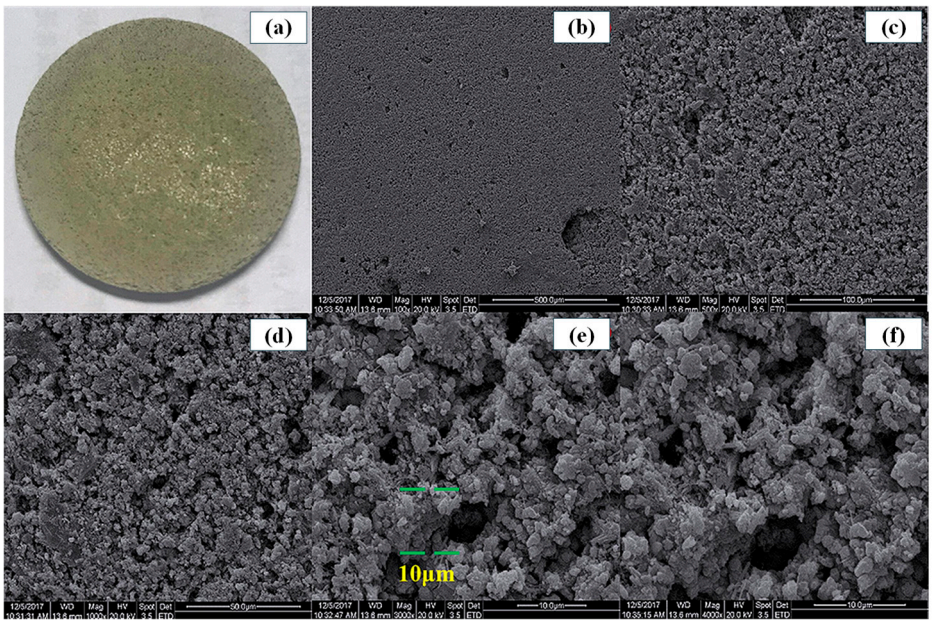

Figure 13. Surface morphologies of the pouring surface at different magnifications [98]. (**a**) the pouring porous wick image. (**b**) ×100. (**c**) ×500. (**d**) ×1000. (**e**) ×3000. (**f**) ×4000.

3.2.4. Carbon-Based Wick

Carbon-based wicks, including those made from carbon foam and biochar, offer promising alternatives for high-performance and environmentally friendly LHP wicks. Silk et al. [103] explored the use of compressed carbon foam wicks, achieving a maximum heat flux of 70 W/cm^2, demonstrating their capability for high-performance heat transfer applications. Liu et al. [104] and Guo et al. [105,106] improved carbon fiber and copper powder wicks through surface modifications to enhance hydrophilicity and thermal performance. These modifications resulted in wicks that started LHPs at lower heat loads and exhibited

minor temperature fluctuations and better temperature uniformity at high loads. These improvements are illustrated in Figure 14a. Brusly Solomon et al. [107] employed natural biochar materials to develop cost-effective and environmentally friendly wicks, reducing the total thermal resistance from 0.75 to 0.17 °C/W across a 50 to 250 W heat input range, as illustrated in Figure 14b. This research demonstrated the potential of biochar wicks to offer economical and performance advantages in thermal management systems. Consequently, biochar is a promising material for future LHP designs.

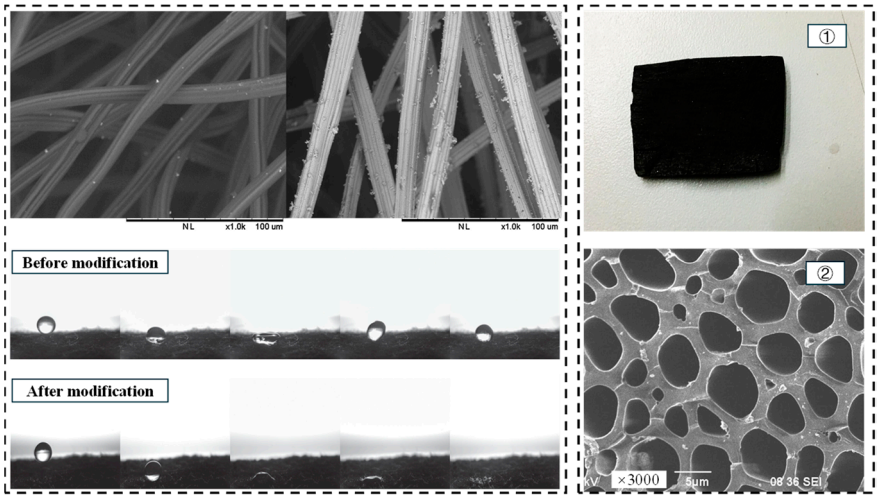

Figure 14. Carbon-based wicks. (**a**) SEM and surface water droplet wettability of PAN-based carbon fiber felt before and after modification [104]; (**b**) Photographic view and SEM image of prepared charcoal: ① Photographic view of prepared charcoal; ② SEM image of Charcoal at 3000×. [107].

In summary, advancements in wick material design have significantly enhanced the thermal performance of LHPs. Metal-based wicks, including those made of copper, zirconia, and stainless steel, have demonstrated improved heat transfer coefficients and reduced thermal resistance through material and structural optimizations. Polymer-based wicks like PTFE provide cost-effective alternatives with high-heat transfer performance and reduced oxidation. Composite and inorganic-based wicks utilize the combined properties of multiple materials to enhance capillary force and minimize dry-out phenomena. Carbon-based wicks such as carbon foam and biochar offer environmentally friendly options with superior thermal management capabilities. Future research should focus on optimizing these materials and exploring new combinations to achieve even greater efficiency and reliability in LHP applications.

4. Loop Heat Pipe Working Fluid

Selecting the optimal working fluid is crucial for the efficiency and reliability of LHPs. The thermophysical properties of the fluid, such as thermal conductivity, viscosity, and specific heat, determine its heat transfer efficiency. Key considerations include the operational temperature range, the fluid's ability to transfer heat during phase changes, and its resistance to gravity and acceleration forces, which can impact performance in various orientations and conditions. Beyond thermal properties, other factors like safety, environmental friendliness, and cost are also important. The fluid should not pose significant health or environmental risks and be economically viable for widespread use. Various organic fluids, such as ethanol and methanol, and inorganic fluids, like ammonia, have been widely studied for their favorable thermophysical properties. Nanofluids, which are fluids with suspended nanoparticles, offer enhanced thermal conductivity and have become a significant area of research. These fluids can potentially improve the heat transfer performance of LHPs significantly. Proper fluid charging levels are also critical, as they ensure

efficient startup and stable operation, balancing rapid heat transfer and minimizing thermal resistance. Overcharging or undercharging can lead to operational inefficiencies or failures. An overview of the research on LHP working fluids is shown in Figure 15, highlighting the various types of fluids studied and their respective impacts on LHP performance.

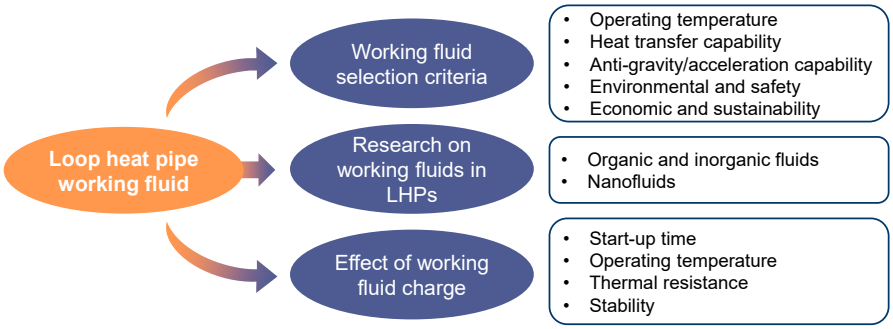

Figure 15. Overview of research on LHP working fluid.

4.1. Working Fluid Selection Criteria

The thermophysical properties of different fluids significantly impact the performance of a heat pipe. These properties include the boiling point, specific heat, latent heat of vaporization, viscosity, and density. The boiling point determines the phase change temperature at a given pressure, which is crucial for designing and operating an LHP. The specific heat, latent heat of vaporization, viscosity, and density collectively determine the fluid's ability to transfer heat within the heat pipe. Consequently, developing a practical methodology for selecting LHP working fluids necessitates comprehensively considering the aforementioned thermophysical properties.

4.1.1. Operating Temperature Range of Working Fluid

The operating temperature range represents the primary consideration when selecting working fluids for LHPs. The working fluid must be able to undergo phase changes between vapor and liquid within this range while maintaining good thermophysical properties throughout. To ensure proper LHP operation, the melting point of the working fluid should be below the lowest operating temperature of the LHP, which the triple point temperature (T_{tri}) can also represent. Additionally, the critical temperature (T_{cri}) should be above the highest operating temperature of the LHP. This precautionary measure prevents the fluid from entering solid or supercritical states within the operating temperature range, thereby ensuring effective heat transfer. For most applications requiring thermal management, such as aerospace electronics and electric vehicles, the optimal and reliable operating temperature range is between −50 °C and 100 °C. Figure 16 compares the two-phase temperature ranges of the typical candidate working fluids for LHPs mentioned in existing studies.

4.1.2. Heat Transfer Capability

The heat transfer capability of the working fluid during the phase change directly impacts the thermal management efficiency of the LHP. This capability is typically quantified as the merit number. The existing literature defines two types of merit numbers, FM_v and FM_l, for the vapor and liquid phases [108–110]. The two merit numbers reflect the working fluid's heat transfer capability in its respective phases. They are represented by Equations (1) and (2), respectively. For the most utilized working fluids in LHPs, the merit numbers within the temperature range of −50 °C to 100 °C are illustrated in Figure 17. A higher merit number signifies a more robust heat transfer capability in the liquid or vapor phase.

$$FM_v = \frac{\rho_v \sigma_l h_{lv}^{1.75}}{\mu_v^{0.25}} \quad (1)$$

$$FM_l = \frac{\rho_l \sigma_l h_{lv}}{\mu_l} \quad (2)$$

where ρ_v and ρ_l represent the densities of vapor and liquid, respectively, σ_l represents the surface tension of the liquid. h_{lv} represents the latent heat of the working fluid. μ_v and μ_l represent the kinetic viscosity of the working fluid, respectively.

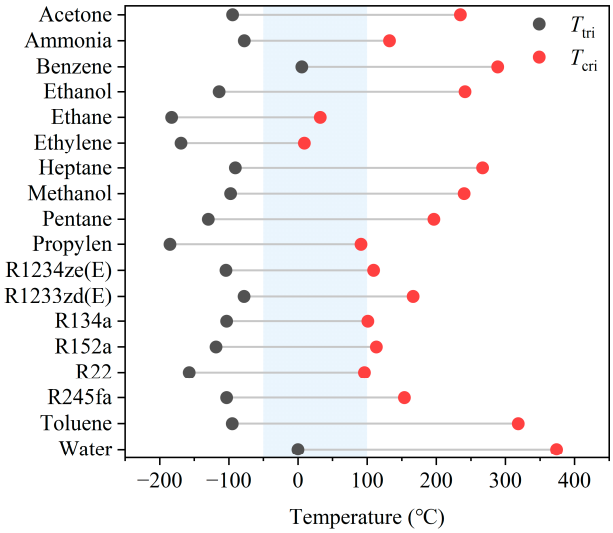

Figure 16. Two-phase temperature range diagram of typical LHP working fluid.

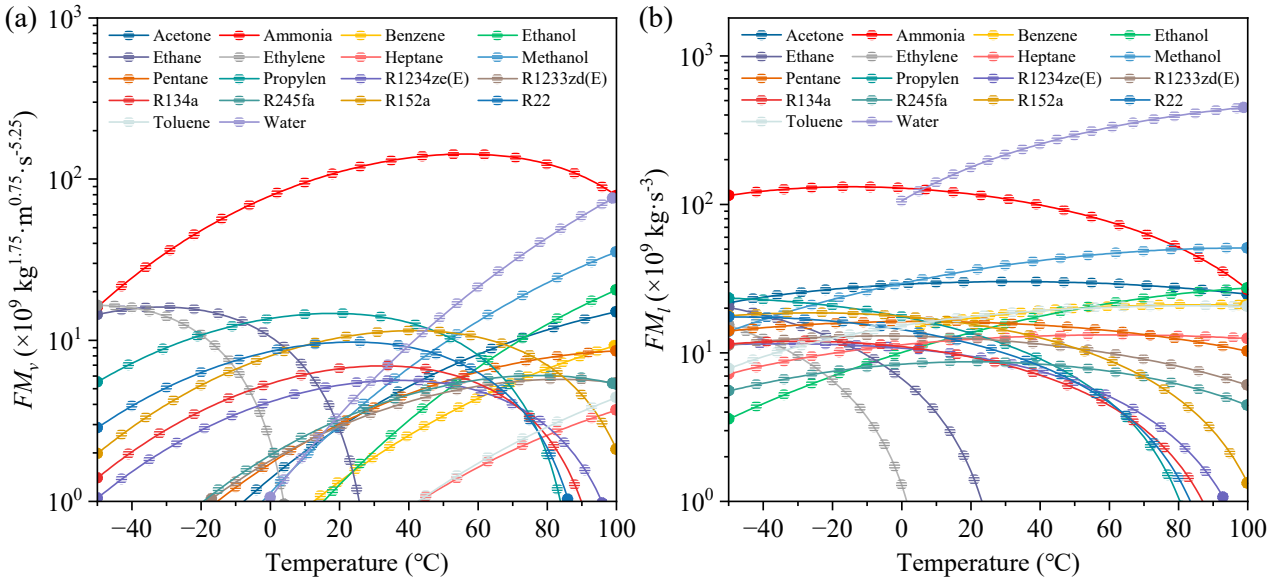

Figure 17. The merit numbers of common working fluids at different temperatures. (**a**) FM_v; (**b**) FM_l.

4.1.3. Anti-Gravity/Acceleration Capability

In aerospace applications, LHPs must perform efficiently under microgravity conditions, where buoyancy-driven natural convection is negligible. Under such conditions, the capillary forces within the porous wick become the primary mechanism for fluid movement. LHPs must also withstand high acceleration forces, where frictional resistance and capillary forces play significant roles in maintaining efficient fluid circulation.

(1) Microgravity performance

Under microgravity conditions, the absence of buoyancy-driven natural convection necessitates reliance on the working fluid's capillary action within the porous wick. The slope of the saturation line on the P-T diagram (dP/dT) is a critical parameter, as a higher

dP/dT value indicates better performance under varying thermal conditions [108,111]. According to Figure 18, Ammonia exhibits the highest dP/dT value across a wide range of temperatures, making it an excellent choice for microgravity environments. Water also demonstrates a significant dP/dT value, especially at lower temperatures, ensuring reliable startup performance.

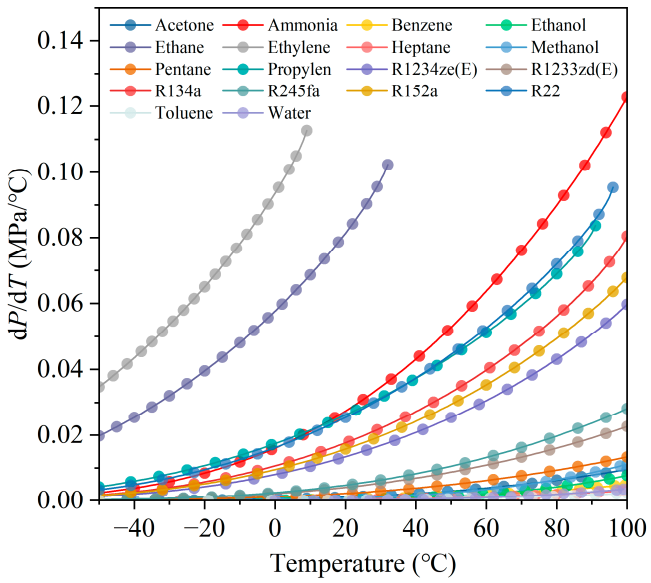

Figure 18. Common working medium at different temperatures (dP/dT).

Other working fluids, such as R1234ze(E), R1233zd(E), and Ethylene, also exhibit favorable dP/dT values. R1234ze(E) and R1233zd(E) provide moderate to high dP/dT values, indicating good adaptability to temperature variations. Ethylene shows promising dP/dT values at lower temperatures, which could benefit specific aerospace applications.

(2) High acceleration resistance

In a high acceleration field, friction from the evaporator to the condenser is the primary resistance to fluid circulation in an LHP. However, the porous wick's capillary force is the main driving force. The resistance increases as acceleration increases, causing the LHP to operate at higher temperatures and reducing its heat transfer capability. Therefore, the ratio of driving force to resistance is a crucial parameter for assessing the impact of acceleration. The higher the ratio, the better the acceleration adaptability. In pertinent studies, $\sigma_l/(\rho_l - \rho_v)$ is employed to quantify this impact [112].

In addition, the saturation pressure of the working fluid plays a pivotal role in limiting the effects of acceleration. For LHPs operating in acceleration fields, the body force induced by acceleration must be considerably smaller than the saturation pressure to prevent circulation termination. Similarly, the saturation temperature and the pressure change caused by acceleration can also be employed to assess the potential acceleration adaptability of the working fluid, expressed as $P_{\text{sat}}/(\rho_l - \rho_v)$ [112]. Figure 19a,b show the $\sigma_l/(\rho_l - \rho_v)$ and $P_{\text{sat}}/(\rho_l - \rho_v)$ for a selection of common working fluids at varying different temperatures.

In summary, for LHPs operating under microgravity and high acceleration conditions, Water and Ammonia emerge as top performers due to their high dP/dT values and strong resistance to acceleration forces, as indicated by their $\sigma_l/(\rho_l - \rho_v)$ and $P_{\text{sat}}/(\rho_l - \rho_v)$ values. Synthetic refrigerants like R1233zd(E) and R1234ze(E) also perform well under these extreme conditions, making them viable alternatives. Other fluids, such as Pentane, Propylene, and Ethylene, demonstrate competitive properties, indicating their potential for effective use in aerospace applications.

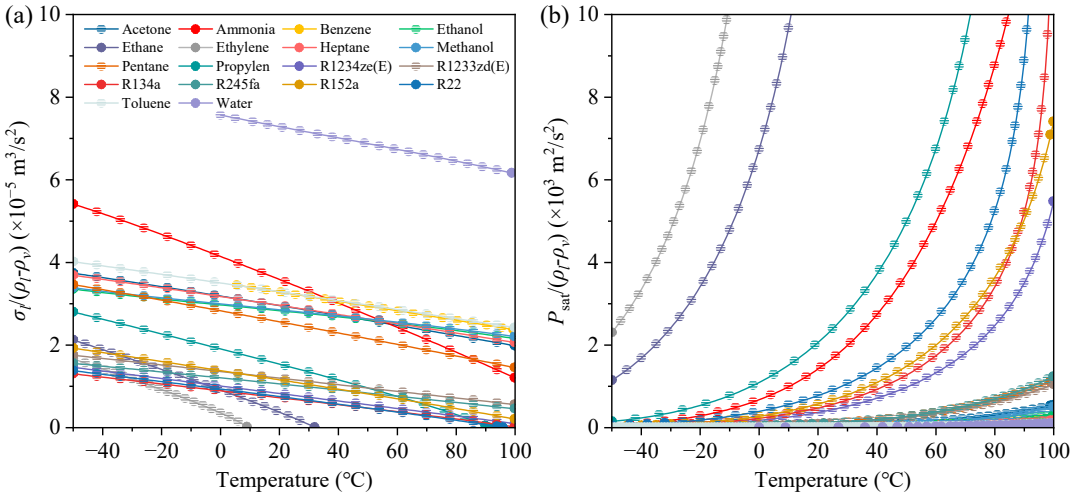

Figure 19. Anti-acceleration parameters of common working fluids at different temperatures. (**a**) $\sigma_l/(\rho_l - \rho_v)$; (**b**) $P_{\text{sat}}/(\rho_l - \rho_v)$.

4.1.4. Environmental, Safety, and Economic Considerations

In addition to thermophysical properties and heat transfer capabilities, the working fluid's environmental friendliness, safety, and economics are key considerations. To this end, this section comprehensively compares common working fluids to toxicity, flammability, regulatory compliance, compatibility with LHP materials, chemical stability, availability, and cost [111].

The aerospace industry has introduced some regulations that make it necessary to consider the environmental friendliness of working fluids [113]. In this paper, the environmental impact of working fluids on the ozone layer and climate change is measured based on the ozone depletion potential (ODP) and global warming potential (GWP), respectively [111]. In addition, the safety of working fluids in LHP applications, including toxicity, flammability, and chemical stability, must be considered [114]. The toxicity of the fluid is critical because highly toxic fluids can significantly increase the health risk to personnel in the event of a spill. Therefore, toxicity is a key criterion for the selection of working fluids. In this paper, based on the lethal dose 50% (LD50) value is used to compare the toxicity of commonly used work fluids, with higher values indicating lower toxicity. Flammability and chemical stability are key, especially in the aerospace and automotive industries [115]. This paper is based on the NFPA 704 flammability rating used to evaluate these metrics. Availability and cost-effectiveness of the working fluid are also key factors. Widely available and economical fluids can be suitable for large-scale LHP applications. Information on working fluids can be accessed through the website https://pubchem.ncbi.nlm.nih.gov. A comparison of commonly used working fluids is shown in Table 1.

From the information in Table 1, it can be concluded that water is the most environmentally friendly option, being non-toxic, non-flammable, and readily available. Toluene, though, has moderate toxicity and a high risk of flammability. R245fa, R22, and R134a are common refrigerants with good performance characteristics. However, R245fa and R134a have a high GWP. Newer refrigerants such as R1233zd(E) and R1234ze(E) have a lower GWP, making them more suitable for environmentally friendly applications, although they are more expensive. Propylene, pentane, and ethylene are flammable, have different toxicities, and must be handled carefully. Methanol, heptane, ethane, and ethanol are also effective, but flammability and compatibility must be considered. Benzene is effective but highly toxic and can cause health problems if leaked. Ammonia is known for its excellent thermal properties but poses a significant safety hazard due to its toxicity and corrosive properties. Acetone is widely used in laboratories and is highly flammable and toxic. In summary, when selecting LHP working fluids, application scenarios should be fully considered, and these factors should be synthesized to screen for the optimal working fluid.

Table 1. Comparison of LHP working fluids in terms of environmental and safety aspects.

Working Fluid	Toxicity (LD50, mg/kg; LC50, ppm/4 h) *	Flammability (NFPA 704 Scale) **	Regulatory Compliance (ODP/GWP)	Compatibility with LHP Materials	Chemical Stability (NFPA 704 Scale) ***	Availability	Cost (USD/kg)
Water	Relatively Harmless, >90,000 mg/kg (oral, rat)	0	0/0	Compatible with most metals and plastics	0	Widely available, used universally	0.96–1.91
Toluene	Slightly Toxic, 8000 ppm (inhalation, rat)	3	0/2.73	Compatible with many metals, limited compatibility with some plastics	0	Readily available, common in the industry	1.05–1.25
R245fa	Practically Non-toxic, >20,000 ppm (inhalation, rat)	1	0/1030	Compatible with most metals and plastics	0	Moderately available, specialized use	17.00–20.00
R22	Relatively Harmless, >250,000 ppm (inhalation, rat)	1	0.05/1760	Compatible with many metals, potential issues with some plastics	0	Limited availability, phased out	6.00–9.00
R152a	Relatively Harmless, 128,000 ppm (inhalation, rat)	4	0/124	Compatible with most materials	0	Readily available, common in HVAC	4.00–6.00
R134a	Relatively Harmless, >500,000 ppm (inhalation, rat)	0	0/1430	Compatible with most metals and plastics	1	Widely available, used in refrigeration	4.50–6.00
R1233zde	Relatively Harmless, 120,000 ppm (inhalation, rat)	0	0/4	Compatible with most materials	0	Moderately available, specialized use	30.00–35.00
R1234zee	Relatively Harmless, >207,000 ppm (inhalation, rat)	1	0/1	Compatible with most materials	0	Moderately available, specialized use	35.00–40.00
Propylene	Practically Non-toxic, >65,000 ppm (inhalation, rat)	4	0/3	Compatible with most metals, potential issues with some plastics	1	Widely available, used in various applications	1.00–1.20
Pentane	Relatively Harmless, 123,361 ppm (inhalation, rat)	4	0/4	Compatible with most metals, limited compatibility with some plastics	0	Widely available, used in labs and industry	1.50–2.00
Methanol	Practically Non-toxic, 64,000 ppm (inhalation, rat)	3	0/0	Compatible with many metals and plastics but can corrode aluminum	0	Widely available, used in industry and labs	0.40–0.50
Heptane	Practically Non-toxic, 48,000 ppm (inhalation, rat)	3	0/0	Compatible with most metals, limited compatibility with some plastics	0	Widely available, common in labs	3.00–4.00
Ethylene	Practically Non-toxic, 57,000 ppm (inhalation, rat)	4	0/0	Compatible with many metals, limited compatibility with some plastics	2	Widely available, used in the industry	1.20–1.40

Table 1. *Cont.*

Working Fluid	Toxicity (LD50, mg/kg; LC50, ppm/4 h) *	Flammability (NFPA 704 Scale) **	Regulatory Compliance (ODP/GWP)	Compatibility with LHP Materials	Chemical Stability (NFPA 704 Scale) ***	Availability	Cost (USD/kg)
Ethane	Relatively Harmless, >800,000 ppm (inhalation, rat)	4	0/0	Compatible with many metals, limited compatibility with some plastics	0	Widely available, common in the petrochemical industry	0.60–0.80
Ethanol	Practically Non-toxic, 50,000 ppm (inhalation, rat)	3	0/0	Compatible with most metals and plastics	0	Widely available, used universally	0.90–1.20
Benzene	Practically Non-toxic, 13,700 ppm (inhalation, rat)	3	0/0	Compatible with many metals, potential issues with some plastics	0	Limited availability, restricted use	1.20–1.50
Ammonia	Slightly Toxic, 2000 ppm (inhalation, rat)	1	0/0	Corrosive to copper and its alloys	0	Widely available, used in the industry	0.30–0.50
Acetone	Highly Toxic, 76 ppm (inhalation, rat)	3	0/0	Compatible with most metals and plastics	0	Widely available, common in labs	1.00–1.20

* Oral LD50 Toxicity Standard (mg/kg, rats): Extremely Toxic: LD50 $\leq$ 1 mg/kg; Highly Toxic: 1 < LD50 $\leq$ 50 mg/kg; Moderately Toxic: 50 < LD50 $\leq$ 500 mg/kg; Slightly Toxic: 500 < LD50 $\leq$ 5000 mg/kg; Practically Non-toxic: 5000 < LD50 $\leq$ 15,000 mg/kg; Relatively Harmless: LD50 > 15,000 mg/kg. * Inhalation LC50 Toxicity Standard (ppm/4 h, rats): Extremely Toxic: LC50 $\leq$ 10 ppm; Highly Toxic: 10 < LC50 $\leq$ 100 mg/kg; Moderately Toxic: 100 < LC50 $\leq$ 1000 mg/kg; Slightly Toxic: 1000 < LC50 $\leq$ 10,000 mg/kg; Practically Non-toxic: 10,000 < LC50 $\leq$ 100,000 mg/kg; Relatively Harmless: LC50 > 100,000 mg/kg. ** NFPA 704 for Flammability scales: 0: Will not burn; 1: Materials that require considerable preheating, under all ambient temperature conditions, before ignition and combustion can occur; 2: Must be moderately heated or exposed to relatively high ambient temperature before ignition can occur; 3: Liquids and solids that can be ignited under almost all ambient temperature conditions; 4: Will rapidly or completely vaporize at normal atmospheric pressure and temperature, or is readily dispersed in air and will burn readily. *** NFPA 704 for Instability–reactivity scales: 0: Normally stable, even under fire exposure conditions; 1: Normally stable, but can become unstable at elevated temperatures and pressures; 2: Undergoes violent chemical change at elevated temperatures and pressures, reacts violently with water, or may form explosive mixtures with water; 3: Capable of detonation or explosive decomposition but requires a strong initiating source, must be heated under confinement before initiation, reacts explosively with water, or will detonate if severely shocked; 4: Readily capable of detonation or explosive decomposition at normal temperatures and pressures.

4.1.5. Lifecycle Analysis for Sustainability of Working Fluid

The evaluation of the sustainability of working fluids necessitates a comprehensive lifecycle analysis, which is of paramount importance for aerospace and vehicular applications [116]. The production phase is concerned with the extraction of raw materials, the manufacturing processes themselves, and the associated energy consumption.

Water is a highly sustainable resource due to its abundant availability and minimal processing requirements, resulting in a low production impact [117]. Producing chemicals such as toluene, pentane, benzene, and hexane derived from petroleum requires significant energy input. This process also generates hazardous byproducts, leading to substantial production impacts. Synthetic refrigerants like R245fa, R22, R152a, and R134a have moderate to high production impacts because their manufacturing processes are energy-intensive [118]. However, newer refrigerants like R1233zd(E) and R1234ze(E) have been developed to be more environmentally friendly, thus reducing their production impact.

The use phase evaluates the working fluid's thermal performance, safety, and economics under various conditions. As mentioned earlier, water has good thermal properties and offers excellent protection. Ammonia has excellent thermal properties but poses safety concerns due to its toxicity. New refrigerants like R1233zd(E) and R1234ze(E) are highly efficient with low global warming potential, making them suitable for aerospace applications [119]. Conversely, though efficient, conventional refrigerants such as R22 and R134a have higher GWPs. Leakage during use can negatively impact environmental sustainability. Due to their flammability and toxicity, toluene, pentane, benzene, and acetone can cause serious safety issues if leaked [120].

The disposal phase of end-of-life working fluids requires particular attention to their environmental impacts and regulatory compliance. As a recyclable resource, water is relatively simple to dispose of and does not present significant disposal challenges, thus ensuring ecological sustainability. Despite the toxicity of ammonia, its waste can fortunately be safely managed through effective neutralization and recovery techniques, reducing the potential threat to the environment. In contrast, the disposal of synthetic refrigerants is more complex and requires specialized treatment methods to prevent them from causing harm to the environment. Fortunately, the newer refrigerants developed in recent years, such as R1233zd(E) and R1234ze(E), have been designed with environmental considerations in mind, aiming to minimize adverse environmental impacts. Toluene, pentane, benzene, and other similar liquids are categorized as hazardous waste, and therefore, strict specifications and careful operating procedures must be followed during disposal. Such disposal processes include using appropriate storage, transportation, and final treatment methods to minimize the potential impact of these substances on the environment and human health [121].

Consequently, water is the most sustainable working fluid for LHPs due to its minimal production impact, high usage efficiency, and minimal environmental footprint. Despite its excellent thermal properties, ammonia requires rigorous safety measures due to its toxicity. Among synthetic refrigerants, R1233zd(E) and R1234ze(E) are favorable options, balancing performance and reducing environmental impact. Fluids such as toluene, pentane, and benzene, which have high production impacts and low safety profiles, are therefore less desirable. Selecting the most sustainable working fluid ensures that LHPs in aerospace applications meet performance requirements under extreme conditions and align with broader environmental and resource efficiency goals. A comprehensive method for selecting working fluids supports the long-term feasibility of aerospace and vehicle technologies while promoting environmental protection.

4.2. Application of Different Working Fluids in Loop Heat Pipes

4.2.1. Organic and Inorganic Fluids as LHP Working Fluid

Organic and inorganic fluids have been extensively studied for their application in LHPs, revealing various performance characteristics that impact heat transfer efficiency. Su et al. [84] highlighted the impact of ethanol–water mixtures. They found that a 60%

ethanol–water mix could reduce the operating temperature to 178.1 °C under a 300 W heat load and decrease the total response time by approximately 26 min compared to pure ethanol. This mixture also demonstrated superior temperature distribution on aircraft wings at −20 °C, indicating its potential to enhance de-icing performance for aviation applications. Similarly, the thermal characteristics of water, methanol, and ethanol as working fluids in copper LHPs were explored by Maydanik et al. [122]. Their study revealed that water could handle a maximum heat load of 900 W with a minimum thermal resistance of 0.020 °C/W. In contrast, methanol and ethanol demonstrated heat transfer capabilities of 380 W and 320 W, respectively, with thermal resistances of 0.015 °C/W and 0.023 °C/W, respectively. These findings underscore the superior heat transfer capabilities of water under high-load conditions. Other organic fluids, including ethane, propylene, and ethylene, were investigated by Liu et al. [112], who found that ethylene-based LHPs exhibited the lowest thermal resistance under identical heat loads, improving performance as operating temperatures increased. This finding suggests that ethylene is particularly effective in reducing thermal resistance and enhancing heat transfer efficiency. Anand et al. [123] investigated the thermal behavior of LHPs with different working fluids (acetone, methanol, n-pentane, and ethanol) under various heat inputs, using visualization of the fluid in the compensation chamber. Results showed that n-pentane had the lowest operating temperature, while methanol had the most comprehensive thermal load range. Notably, n-pentane performed best in heat dissipation applications as low as 115 W.

Ammonia has also been a research focus due to its favorable thermodynamic properties. The performance of an ammonia-based LHP with mechanical pump assistance was presented by Zhang et al. [124], demonstrating stable start-up within 5 min and no temperature overshoot or oscillation during dynamic heat load responses. Ammonia has higher saturation pressure and more excellent latent heat of evaporation-enhanced performance than methanol-based LHPs. Furthermore, Jasvanth et al. [125] employed anhydrous ammonia in high-power spacecraft thermal management, demonstrating remarkable performance under diverse heat loads and adverse height conditions. Their ammonia-based LHP achieved an evaporative heat transfer coefficient exceeding 15,000 W/m^2K and maintained stable operation even at an adverse height of 1000 mm.

The application of environmentally friendly refrigerants has also been explored. Zhao et al. [126] investigated using R1233zd(E), a fourth-generation refrigerant known for its ultra-low toxicity and non-flammability. Despite its relatively minor latent heat compared to traditional fluids, R1233zd(E) demonstrated stable operation under harsh conditions, maintaining a minimum thermal resistance of 0.197 °C/W at a heat sink temperature of 0 °C. The fluid's ability to prevent liquid droplets in vapor lines and ensure stable operation under various environmental conditions renders it a viable option for LHPs. Xu et al. [113] evaluated two new refrigerants, R1234ze(E) and R245fa, demonstrating that R1234ze(E) exhibited a superior start-up response, while R245fa exhibited more robust heat transfer capabilities. At optimal filling ratios of 65% to 70%, R1234ze(E) maintained characteristic temperatures below 35 °C with thermal resistance between 0.08 K/W and 1.62 K/W under 5 W to 40 W heat loads. Conversely, R245fa demonstrated optimal performance with thermal resistance ranging from 0.18 K/W to 0.91 K/W under 10 W to 60 W heat loads, maintaining operating temperatures below 60 °C. Additionally, R134a, a refrigerant with a well-established reputation for efficiency, has been extensively studied in LHP applications, exhibiting effective thermal management and operational stability in a range of conditions [127–129].

4.2.2. Nanofluids as LHP Working Fluid

Nanofluids have emerged as a promising working fluid category for LHPs, enhancing thermal performance by adding nanoparticles. These nanoparticles improve thermal conductivity and heat transfer properties, offering significant performance enhancements over conventional fluids. The performance enhancements provided by silicon–water nanofluids were documented by Jose et al. [130], who found that a 2% nanoparticle concentration re-

duced the evaporator temperature by 27% and decreased the time to reach a steady state by 150 s compared to deionized water. This finding demonstrates the potential of nanofluids in reducing thermal resistance and enhancing the overall efficiency of LHP systems.

In a comparative study conducted by Stephen et al. [131], the addition of 0.12 vol% Ag nanoparticles to Al_2O_3/water nanofluids was found to reduce evaporator thermal resistance by 34.70% and increase convective heat transfer coefficients by 34.52%. This result demonstrated that the Ag nanoparticles were more effective than Al_2O_3/water nanofluids in enhancing heat transfer. The benefits of copper oxide nanofluids were further explored by Zhao et al. [132], who demonstrated that these nanofluids increased the maximum heat load from 290 W to 310 W and reduced the minimum start-up heat load from 40 W to 20 W. 12.7 °C reduced the evaporator wall temperature and the evaporator thermal resistance decreased by 26.9%, indicating substantial performance gains.

The positive impact of copper nanoparticles in water-based nanofluids on mLHPs was demonstrated by Wan et al. [133]. The researchers found that these nanofluids reduced evaporator wall temperatures and overall thermal resistance, attributing this to the improved boiling heat transfer and increased capillary force provided by the nanoparticles. Harun et al. [134] investigated various nanofluids, including diamond, alumina, and silica. Their findings indicated that diamond nanofluids exhibited the most significant thermal enhancement at a concentration of 1.19%, reducing a reduction in thermal resistance and an improvement in heat capacity. Aun et al. [135] showed that even low concentrations of diamond nanoparticles in water enhanced heat transfer efficiency, reduced bubble size, achieved a faster steady state, and lowered total thermal resistance. These findings substantiate the efficacy of diamond nanofluids as high-performance LHP working fluids.

Further research by Gunnasegaran et al. [136,137] and Tharayil et al. [138] has corroborated the benefits of nanofluids. Silica–water nanofluids reduced total thermal resistance by 28% to 44% across various heat inputs, while graphene-water nanofluids, even at low concentrations, lowered thermal resistance and improved system responsiveness. These findings indicate the potential of nanofluids to advance LHP technology, offering superior thermal management and operational stability. Consequently, they represent a promising avenue for enhancing the performance of LHP systems.

4.3. The Effect of the Charge of Working Fluid

The charge of the working fluid in LHPs can influence their operational performance, thermal resistance, and stability. Adoni et al. [139] emphasized that the amount of liquid in the compensation chamber critically affects LHP operation. Their study indicated that an excessive liquid charge in the compensation chamber could disrupt the thermal coupling between the compensation chamber and the evaporator core, leading to a monotonous increase in operating temperature underground conditions. This insight was echoed by Mo et al. [140], who observed that undercharged conditions in cryogenic LHPs (CLHPs) led to unique thermal behaviors, such as temperature oscillations at low power levels and a notable impact on thermal resistance and performance in different orientations. Nagano et al. [141] further highlighted the importance of appropriate charge levels, showing that insufficient working fluid charge can cause start-up failures while overcharging reduces LHP stability. Their experiments underscored the pivotal role of charge levels in ensuring reliable start-up and transient behavior. Wang et al. [142] demonstrated that in mLHPs, the working fluid charge can affect start-up time and operating temperature. Lower charges facilitate quicker start-ups but result in higher operating temperatures, while higher charges result in longer start-up times but more stable, lower operating temperatures.

In their investigation of copper–water LHPs, Zhang et al. [143] discovered that a higher working fluid charge effectively minimizes thermal leaks and maintains the capillary structure's wettability at low-heat loads. Their experiments indicated that an optimal charge level of approximately 70% balances rapid start-up and high-heat transfer capacity while minimizing thermal resistance. Conversely, overcharging, at 78.3%, induced strong temperature oscillations and increased thermal leaks during operation. Armijo et al. [134]

investigated a binary mixture with a strong Marangoni effect. It was found that a 45% liquid filling ratio optimized critical heat flux conditions and reduced evaporator wall superheat. Smitka et al. [144] demonstrated that for electronic component cooling, an optimal fluid charge of 60–70% provided the best cooling performance, maintaining the temperature of insulated-gate bipolar transistors (IGBTs) under 100 °C at a 400 W load, while an 80% charge led to performance decline and overheating even at lower loads. Blauciak et al. [145] further corroborated these findings by demonstrating that different fluid charges affect pressure differentials and mass flow rates in LHPs. Specifically, a 65 mL charge yielded the highest-pressure differential.

Furthermore, Singh et al. [111] examined the effects of working fluid charge under various operating orientations. They concluded that a 40–60% charge range optimized LHP performance, with 50% providing the best thermal performance across most conditions. The study underscored the influence of fluid charge on start-up characteristics and steady-state performance, as well as the distribution of the working fluid within LHP components, which affects operational temperatures and thermal resistance. D'Entremont et al. [146] supported these findings, revealing that partially filled compensation chamber s (Partial-CC) enhance start-up behavior, temperature regulation, and thermal conductance by improving condenser utilization and minimizing hysteresis during phase transitions. Song et al. [147] further noted that precise control of the fluid charge in silicon-based ultra-thin LHPs (s-UTLHPs) allows for rapid start-up and stable operation under high-heat fluxes, preventing dry-out scenarios and maintaining efficient thermal management in microchip cooling applications. These studies emphasize the critical role of optimizing working fluid charge to enhance LHP performance across different applications and operational conditions.

5. Optimization of Loop Heat Pipe Operational Characteristics

The optimization of LHP operation involves key aspects such as start-up behavior, temperature oscillation phenomena, and NCG. Operational conditions and design parameters significantly influence the start-up behavior of LHPs, determining their efficiency and reliability. A successful start-up involves the rapid and stable formation of the vapor phase in the evaporator and the subsequent circulation of the working fluid throughout the system. Delays or instability during start-up can lead to inefficiencies or failure to initiate proper heat transfer. Temperature oscillations occur due to complex interactions between the vapor and liquid phases within the LHP components, such as the evaporator, condenser, and compensation chamber. These oscillations can lead to fluctuations in the temperature of the working fluid, affecting the stability and efficiency of the heat transfer process. Mitigating temperature oscillations involves implementing design adjustments, such as optimizing the wick structure to refine the evaporator's and condenser's geometry. NCGs are detrimental to LHP performance, particularly during the start-up and operational phases. NCGs can accumulate in the system, causing blockages and pressure build-up that hinder the flow of the working fluid. This results in increased thermal resistance and reduced heat transfer efficiency. By addressing these factors, the performance of LHPs can be significantly enhanced, making them more effective for applications in aerospace, high-power electronics, and new energy vehicles. Figure 20 provides an overview of research on the operating characteristics of LHPs, highlighting the critical areas of focus for optimizing their performance.

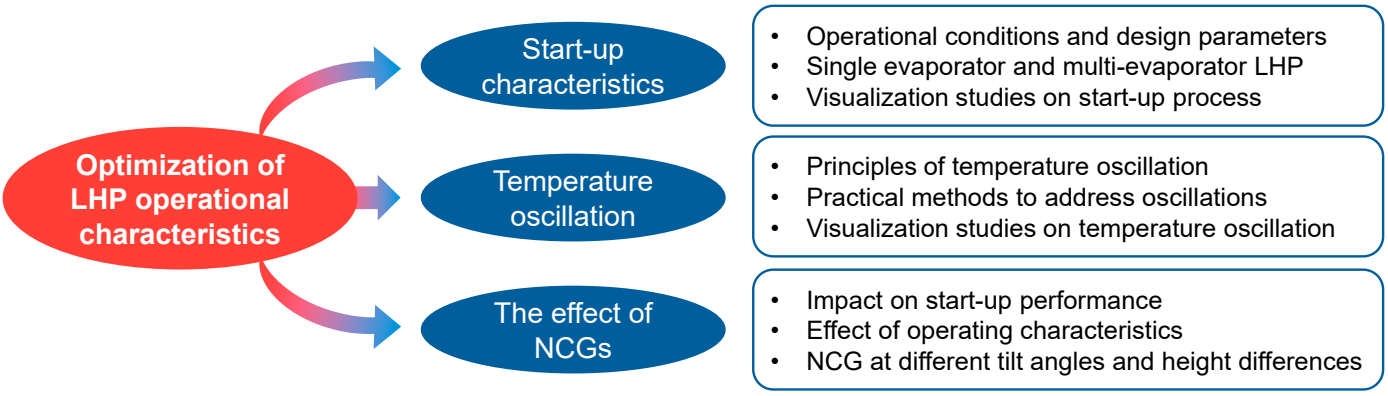

Figure 20. Overview of research on operating characteristics of LHPs.

5.1. Start-Up Characteristics

The operational conditions and design parameters that influence the start-up behavior of LHPs are numerous and complex. Zhang et al. [148] conducted comprehensive ground experiments to explore the impact of different working conditions on the start-up characteristics of LHPs, focusing on parameters such as vapor/liquid distribution in the evaporator, start-up heat load, sink temperature, and adverse heights. They observed that the evaporator filled with liquid at low start-up heat loads can lead to evaporation within the fibers, along with temperature oscillations at the condenser inlet and reverse flow balance, resulting in higher operating temperatures. This observation aligns with findings from Rodriguez et al. [149], who studied the transient characteristics during LHP start-up, particularly when a large mass is attached to the evaporator. The results indicated that temperature overshoots occurred due to the initial high temperature required to start the LHP. Additionally, the study discussed the beneficial use of start-up heaters to mitigate these issues, highlighting the complex interplay between mass and thermal dynamics during the start-up phase.

The findings of Lu et al. [150] indicate that LHPs require longer start-up times at low-heat loads due to the necessity of sufficient capillary pressure to circulate the working fluid. In contrast, high-heat loads facilitate quicker start-ups. This phenomenon indicates that LHPs start more easily under higher heat loads, accelerating the capillary action necessary for efficient fluid circulation. In addition, Bai et al. [151,152] examined DCCLHP, revealing that they reliably start at low-heat loads, although sometimes with high-temperature overshoots. The thermal load and resistance between the evaporator and compensation chamber can influence their performance. These findings underscore the importance of optimizing thermal resistance and load distribution for effective start-up. Chernysheva et al. [153] provided further insights using numerical simulations to study LHP start-up with a fully liquid-filled system. This study highlighted the critical impact of geometric parameters, material thermal properties, and heat load on temperature field formation and start-up success, especially at low-heat loads.

The impact of various design features on start-up characteristics has been extensively investigated. Huang et al. [25] classified LHP start-up phenomena into four modes based on heat load: failure, oscillation, overshoot, and routine. These behaviors were particularly pronounced at lower heat loads, with overshoot and oscillation observed at loads below 40 W and between 20 W and 40 W, respectively. This classification facilitates the practical design and optimization of LHPs by providing a framework for predicting and managing start-up behavior. Wang et al. [154] found that increasing the thickness of the sintered capillary layer inside the heat pipe improved start-up performance by reducing heat leakage to the compensation chamber and enhancing the temperature differential between the chamber and the evaporator. Meanwhile, Bai et al. [155] demonstrated that FLHPs outperform traditional cylindrical evaporators, particularly at low-heat loads as low as

2 W. Furthermore, they exhibited simpler start-up processes and minimal temperature overshoots in horizontal and vertical positions.

In addressing the difficulties encountered when initiating the operation of LHPs under certain conditions, Hoang et al. [156] proposed using electric heaters or thermoelectric coolers to ensure reliable start-up, even when operating at low power inputs or when connected to large thermal masses. Their approach emphasized the importance of understanding the theoretical and practical aspects of start-up issues and designing pre-set start-up procedures to ensure reliable operation. Boo et al. [157] introduced an improved method by installing a bypass line between the evaporator and liquid reservoir, reducing the minimum heat load required for start-up by 37%, enhancing reliability and efficiency. Ji et al. [86] examined LHPs with composite multi-scale porous coatings, which reduced start-up time, lowered wall temperatures, and suppressed temperature instabilities. The dual sintering of various particle sizes resulted in the formation of effective vapor release and liquid absorption channels, which improved the start-up performance and thermal efficiency of the coatings under different tilt angles and fill ratios. Wang et al. [158] additionally examined the dynamic response of LHPs during start-up with varying heat sink temperatures. Their findings indicated that higher auxiliary start-up power facilitated easier initiation and stabilized the vapor–liquid interface in the condenser, thereby ensuring a more seamless transition to steady-state operation.

The start-up characteristics of DE-LHPs have also been studied for their unique behavior and performance. Qu et al. [79] found that factors such as vapor–liquid distribution in the evaporators, the interaction between the two evaporators, heat load distribution, and core material sealing affect start-up performance. DE-LHPs performed best when both evaporators had equal heat loads, with vapor in the vapor grooves and liquid in the evaporator cores. This balanced distribution allows for optimal start-up conditions. He et al. [80] confirmed these findings by demonstrating that dual evaporator LHPs can start and operate effectively under different heat load distributions and maintain stability even under unbalanced conditions. Despite the interaction between the evaporators affecting the start-up performance, effective cooling of both heat sources was achieved without interference through careful design. This result highlights the potential for dual evaporator systems to improve thermal management efficiency.

Visual studies have provided more profound insights into the LHP start-up process, revealing intricate details of fluid behavior. Wang et al. [159] performed visual experiments showing that start-up is driven by capillary action and vapor pressure in the boiling pool. They observed a "breathing phenomenon" where increasing the heat load of the boiling pool accelerated start-up but caused significant overheating. This visual approach helped to identify the dynamic transitions within the LHP during start-up. Nishikawara et al. [160] used optical observations to study the liquid–vapor behavior in capillary evaporators during start-up. They found that the liquid–vapor distribution affected the temperature curve but not the steady-state characteristics, as depicted in Figure 21. They identified four transient behaviors: boiling in the compensation chamber and liquid surface oscillation. They provided visual evidence to understand the relationship between start-up characteristics and initial phase distribution in LHPs. This insight aids in developing models and clarifying transient behavior associated with capillary evaporators, adding a crucial dimension to the study of LHP start-up processes and improving the predictability and reliability of these systems in practical applications.

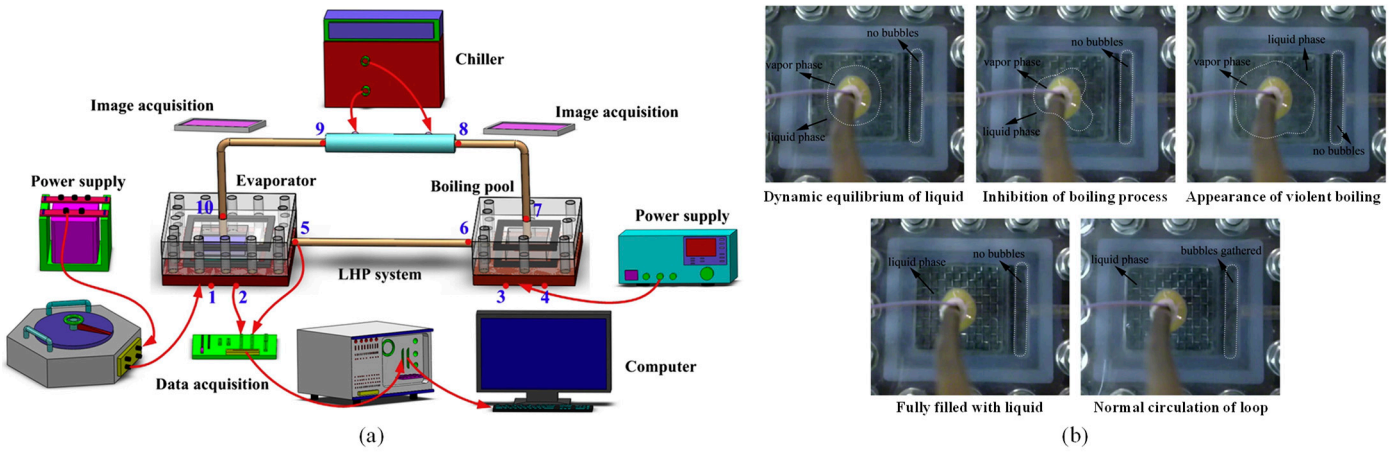

Figure 21. (**a**) Scheme of the experimental setup and the arrangement of thermocouple positions (1–10). (**b**) Work fluid behavior changes in the compensation chamber and the vapor chamber during the startup process [159].

5.2. Temperature Oscillation Phenomenon

The underlying principles of temperature oscillations in LHPs have been studied extensively, revealing the complex interactions and dynamics that give rise to these phenomena. Ku et al. [128] first identified high-frequency, low-amplitude temperature oscillations. They found that these oscillations result from the failure of the vapor front in the condenser to stabilize, causing it to oscillate near the condenser's inlet or outlet. This instability is driven by the rapid movement of the vapor front, which cannot find a stable position under certain operating conditions. Building on this, Ku et al. [161] proposed that low-frequency, high-amplitude oscillations occur due to the complex interaction between the compensation chamber, condenser, thermal mass, and environment, especially when the LHP is connected to a large thermal mass with low-heat load and very low condenser temperature. This interaction causes oscillating heat input to the evaporator that correlates with the movement of the steam front in the condenser, resulting in temperature oscillations. Singh et al. [162] extended this research by investigating temperature oscillations in mLHPs under varying heat loads. They found that oscillations occurred in the 10–20 W range, driven by heat leakage from the evaporator to the compensation chamber and fluctuations in condensate temperature. Despite these oscillations, the mLHPs maintained effective heat transfer performance, demonstrating their robustness even under challenging conditions.

Furthermore, Li et al. [64] studied LHP start-up and steady-state operation under different heat loads. They found that irregular temperature oscillations at lower loads were mainly due to intermittent steam bubble formation, collapse, and instability in the condenser. These oscillations gradually diminished as the heat load increased, resulting in stable operation at higher loads. In a comparative study, Celata et al. [163] found that LHPs exhibited more pronounced temperature and pressure oscillations under unfavorable conditions (evaporator above the compensation chamber) due to NCGs and unfavorable gravitational effects. In contrast, favorable conditions (evaporator below the compensation chamber) resulted in stable operation without oscillations. Zhang et al. [164] and Liu et al. [165] also found that inadequate fluid distribution in the compensation chamber and thermodynamic interactions between the evaporator, compensation chamber, and condenser at low-heat loads contribute to temperature oscillations. Hoang et al. [166] proposed a theory based on the stability of nonlinear dynamic systems, explaining that temperature oscillations arise when the system bifurcates into a periodic but stable state after exceeding critical parameters. They detailed how phase change heat/mass transfer and fluid dynamics within various LHP components collectively cause temperature oscillations. These studies collectively highlight the crucial role of optimizing fluid dynamics and distribution to stabilize LHP operation and mitigate oscillations. Feng et al. [167] investigated the

operational instabilities, including temperature oscillations in DCCLHPs, noting that these oscillations often occur during power cycling tests and are more pronounced when the compensation chamber is above the evaporator. Lv et al. [168] studied the effects of acceleration forces on DCCLHPs and found that increased acceleration exacerbates temperature oscillations, especially at higher heat loads, due to dynamic interactions between acceleration forces and thermal management processes. Yerkes and Scofield [169] added that acceleration forces can either enhance or interfere with thermodynamic drivers, potentially triggering or mitigating temperature oscillations depending on the operational context.

Visualization studies have provided critical insight into the phenomenon of temperature oscillation in LHPs, highlighting the dynamic fluid behaviors contributing to these phenomena. Mo et al. [170] used flow visualization to show that temperature oscillations occur even at constant heating power, particularly at the condenser outlet. These oscillations were categorized into small and large amplitude types, with small oscillations persisting with increasing energy, while large oscillations initially disappeared but later reappeared. Zhang et al. [171] conducted similar studies under different tilt angles and found that oscillations arise from the vapor–liquid interface and pressure oscillations within the coupled evaporator-compensation chamber structure. These oscillations can affect fluid flow and temperature distribution within the LHP. Liu et al. [172] investigated a novel LHP with a vapor-driven jet injector. They observed high-amplitude oscillations due to intermittent liquid supply to the compensation chamber, as shown in Figure 22. These oscillations were mitigated by adjusting the fill ratios and heat sink temperatures, resulting in more stable operation. Li et al. [173] linked different types of oscillations to flow patterns in the condenser and showed that high thermal conductivity materials helped reduce oscillations by stabilizing the flow. Recently, Du et al. [174] visualized temperature oscillations and two-phase behavior in flat LHPs and found that higher fill ratios reduced oscillations, which were more pronounced during the boiling and stabilization phases.

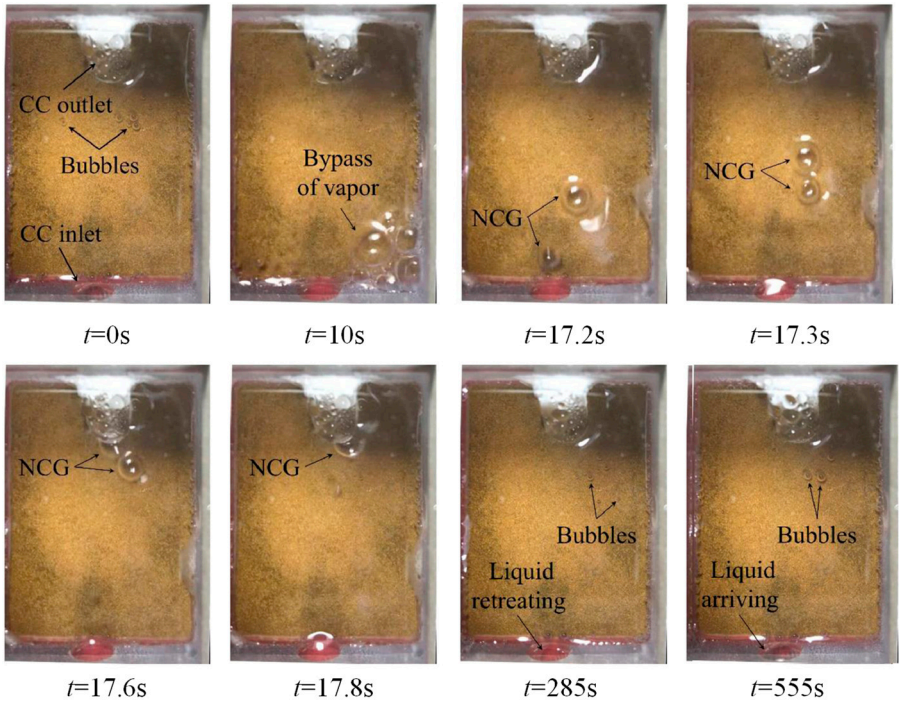

Figure 22. Working fluid behavior in the compensation chamber within an oscillation period [172].

Several practical applications have demonstrated methods to address these oscillations. Chen et al. [175] showed that dual-pore capillary structures in flat plate evaporators reduced temperature oscillations, especially at heat loads below 5 W. These structures provided stable performance at higher loads by minimizing heat loss to the compensation

chamber. Liu et al. [176] found that while LHPs exhibited stable operating temperatures at low- and high-heat loads, persistent temperature oscillations often occurred due to unstable seals between the evaporator inlet and the compensation chamber. This instability could be addressed by charging the fill ratio or adjusting the heat sink temperature, which improved the heat transfer coefficient and reduced the oscillation characteristics. Mo et al. [177] studied temperature oscillations in FLHPs under different gravitational orientations and identified temperature overshoots and high-frequency, high-amplitude oscillations at low-heating power in vertical orientations. As the heat load increases beyond 300 W, the loop thermal resistance decreases to a minimum of approximately 0.2 K/W in the vertical orientation assisted by gravity. Zakar et al. [178] extended this by theorizing that LHPs function as dynamic systems influenced by external conditions and classified oscillations into high-frequency low-amplitude (HFLA) and low-frequency high-amplitude (LFHA) types. Xu et al. [179] examined the effect of different fill ratios on temperature oscillations in flat copper-water LHPs and found that low fill ratios led to evaporator drying and oscillations. At the same time, high fill ratios also induced frequent oscillations at low-heat loads. Intermittent backflow from the condenser was noted at 40% and 60% fill ratios, causing temperature oscillations at low-heat loads (30 and 40 W). At a fill ratio of 40%, inadequate inventory led to evaporator dry-out; at 60%, excessive backflow reduced superheat. An optimal fill ratio of 50% balanced thermal leakage and oscillations, ensuring efficient and stable heat transfer up to 120 W. Adachi et al. [26,51] developed a transient model linking temperature oscillations to two-phase flow in the liquid line. They also suggested adjusting the heat capacity of the reservoir or direct heating to prevent oscillations by maintaining a significant temperature difference.

5.3. The Effect of Non-Condensable Gas

The presence of NCG can affect the start-up and operating characteristics of LHPs. Hus et al. [180] highlighted that NCG in mLHPs can block tiny pathways, leading to excessive pressure build-up and potential wick breakage. This study emphasized the need for effective NCG removal during the design and testing stages to ensure optimal operation. Singh et al. [181] observed that NCGs form primarily during the initial thermal cycles and accumulate in the compensation chamber, increasing overall system pressure and prolonging the evaporator's start-up time. Despite this, mLHPs showed higher tolerance to NCGs due to the compensation chamber's ability to absorb most of the released gases without performance degradation. They suggested improved cleaning and degassing procedures to mitigate NCG formation.

Prado-Montes et al. [182] explored a LHP operating at temperatures up to 125 °C. The operational impact was minimal, even with NCG levels exceeding the expected amount at the end of the satellite's life. They noted discrepancies between experimental results and simulations, likely due to NCG circulating with the working fluid or being absorbed by materials rather than remaining in the compensation chamber. Maydanik et al. [183] studied high-capacity LHPs after long-term storage. They found that LHPs with stainless steel and ammonia or water as working fluids retained their thermal performance for nearly 30 years, suggesting that small amounts of NCG do not affect performance, especially at higher heat loads. He et al. [184] studied the partial pressure of NCG in the compensation chamber and found that NCG increased the evaporator's operating temperature, especially at low-heat load or sink temperature, and caused unique temperature oscillations. They analyzed these oscillations' physical mechanisms, which were less common in previous research. In further studies, He et al. [27] evaluated the effect of NCG on LHP start-ups under various conditions and found that higher amounts of NCG degraded start-up performance.

In contrast, higher start-up heat loads improved it. The presence of NCG in the evaporator's vapor groove was noted to promote liquid evaporation, potentially facilitating ideal start-up conditions. Anand [185] focused on the effect of NCG when using low-pressure working fluids and proposed a novel method to estimate the mass of NCG in the compensation chamber and its impact on the deprime phenomenon. The study revealed

that the presence of NCG increases operating temperatures, reduces heat transfer capacity, decreases capillary pressure, and increases evaporative droplet radius, thus negatively affecting overall LHP performance.

NCG affects the performance of LHPs at different evaporator slopes and relative heights of the evaporator and condenser. Wang et al. [186] investigated the start-up performance of LHP with NCG at different evaporator tilt angles, as shown in Figure 23a. They found that LHPs could operate normally with NCG at small tilt angles. In contrast, a successful start-up was only possible with minimal NCG at larger tilt angles. Large amounts of NCG prevented start-up regardless of the tilt angle. Wang et al. [187] further investigated the coupled effects of NCG and evaporator tilt angles, as illustrated in Figure 23b, and found that NCG increased steady-state operating temperatures under all tilt conditions. However, the temperature increase was less pronounced at unfavorable tilt angles (evaporator above compensation chamber). At a tilt angle of 0°, the evaporator outlet temperature difference decreased from 8.4 °C to 3.7 °C as the heat load increased from 15 W to 135 W. At a tilt angle of −15°, it remained around 4.6 °C across the heat load range. A tilt angle of 15° ranged between 1.1 °C and 4.0 °C, even though the overall temperatures were higher. They emphasized the importance of considering these interactions in the ground applications of LHPs. Wang et al. [188] extended this investigation to include the impact of evaporator/condenser height differences on LHP performance with NCG, as depicted in Figure 23c. They discovered that NCG resulted in temperature increases, but the trends varied with the relative height. At zero and adverse elevations, the temperature rise due to NCG negatively correlates with heat load, peaking at 6.8 °C and 4.1 °C at 15 W, respectively. Under favorable elevation, the rise is positively correlated with heat load in gravity-driven mode and negatively in capillarity-gravity co-driven mode, with a maximum of 4.8 °C at 60 W. In addition, the presence of NCG and unfavorable altitudes improved reflux during startup, thereby increasing stability.

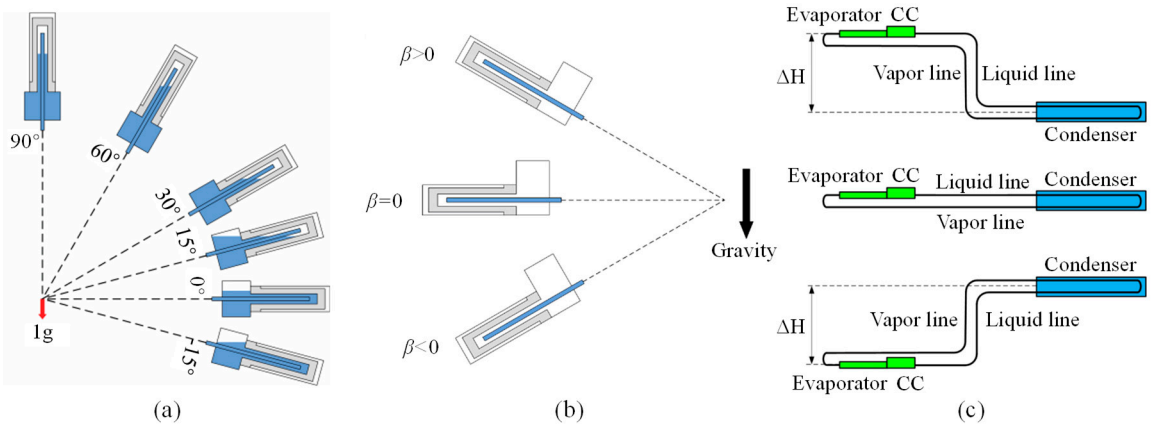

Figure 23. Diagram of the tilt angle of the evaporator and the relative position of the evaporator/condenser. (**a**) Schematic of evaporator tilt angle [186]; (**b**) Schematic of the tilt angle of the evaporator [187]; (**c**) Schematic of the various evaporator/condenser elevations [188].

Efforts to mitigate the adverse effects of NCG on LHP performance have focused on material selection and technological interventions. Hartenstine et al. [189] demonstrated that using titanium in LHPs reduced NCG production compared to conventional aluminum and stainless steel. Titanium's compatibility with water at high temperatures, low density, high strength, and advantageous low thermal conductivity to minimize heat leaks improved LHP reliability and efficiency. Yang et al. [190] explored the application of TEC in LHPs with NCG, finding that TECs could markedly improve thermal performance by lowering steady-state temperatures, expanding allowable heat loads, ensuring successful start-up, reducing temperature overshoot, and eliminating or suppressing potential temperature oscillations. They provided design considerations for TEC components to optimize their

role in enhancing the thermal performance of NCG-affected LHPs, providing crucial insights for future long-lived space thermal control systems based on LHPs.

6. Conclusions and Outlook

The demand for efficient thermal management systems has become increasingly urgent due to breakthroughs in various areas. In this context, LHPs have emerged as ideal solutions for high-temperature, high-heat flux, high-power dissipation, and complex thermal management scenarios due to their excellent heat transfer performance, reliability, and flexibility. This paper provides a systematic review and in-depth analysis of the critical technologies of LHPs. The main conclusions are as follows:

(1) Research on LHP thermohydraulic behavior has advanced by establishing steady-state and transient models. Steady-state models improve computational efficiency and predict LHP performance, while transient models capture dynamic behavior for start-up and non-steady-state evaluations. Future research should refine these models to incorporate practical conditions and enhance accuracy. Additionally, developing more efficient transient models to reduce computational time is crucial.

(2) Component design is crucial for enhancing LHP thermal performance. Research focuses on optimizing evaporators and compensation chambers, with single-evaporator designs emphasizing compactness and efficient start-up, while multi-evaporator designs offer flexibility for complex environments. Innovations in wick materials, including porous metals, composites, and 3D printing, improve capillary driving force and heat transfer. Future research should explore new materials and structures to increase efficiency and reduce thermal resistance, while also ensuring long-term stability and durability under extreme conditions.

(3) The thermophysical properties of the working fluid significantly impact LHP performance. It is essential to evaluate factors like thermal properties, anti-gravity capability, environmental friendliness, safety, and economy when selecting the fluid. Water offers high efficiency due to its latent heat of vaporization, good thermal conductivity, and non-toxicity. Ammonia is ideal for low temperatures and performs well under microgravity. Nanofluids enhance heat transfer and stability. Future research should focus on exploring novel or mixed working fluids to further optimize LHP performance.

(4) Research on the start-up performance and temperature oscillation phenomena of LHPs has highlighted the system's complexity and optimization potential. Optimizing vapor/liquid distribution, heat load, and sink temperature can improve start-up efficiency and minimize temperature overshoot. Temperature oscillations arise from thermodynamic and fluid dynamic interactions. Enhancing capillary structures and optimizing working fluid properties significantly reduce these oscillations. Future research should focus on optimizing start-up processes and reducing temperature oscillations in multi-evaporator LHPs to enhance system stability.

(5) NCGs affect LHP start-up and operating characteristics by increasing evaporator temperatures, causing temperature oscillations, and raising thermal resistance, thus reducing heat transfer efficiency. Selecting appropriate materials like titanium and using technical interventions such as thermoelectric coolers can mitigate these effects. Future research should focus on NCG generation and control mechanisms and develop efficient degassing techniques to ensure the long-term stability and reliability of LHPs.

Although LHP technology has significant potential in thermal management applications, it still faces many challenges. Future research should continue to refine thermohydraulic modeling, optimize component design, wick material design, and working fluid selection, and explore new materials and technologies to enhance the heat transfer performance and operational stability of LHPs. Moreover, system-level integration and optimization, especially in complex thermal management environments, will support the widespread adoption of LHP technology. Through continued technological innovation, LHPs are expected to play a critical role in a broader range of applications, driving further development in thermal management technology.

Author Contributions: Conceptualization, M.W.; investigation and resources Y.Z.; writing—original draft preparation Y.Z.; writing—review and editing, M.W. and D.D.; supervision, M.W.; funding acquisition M.W. and D.D. All authors have read and agreed to the published version of the manuscript.

Funding: This research was funded by National Natural Science Foundation of China, grant numbers 52376043 and 52202434.

Data Availability Statement: No new data were created or analyzed in this study. Data sharing is not applicable to this article.

Conflicts of Interest: The authors declare no conflicts of interest.

References

1. Dan, D.; Zhao, Y.; Wei, M.; Wang, X. Review of Thermal Management Technology for Electric Vehicles. *Energies* **2023**, *16*, 4693. [CrossRef]
2. Maydanik, Y.; Pastukhov, V.; Chernysheva, M. Development and investigation of a loop heat pipe with a high heat-transfer capacity. *Appl. Therm. Eng.* **2018**, *130*, 1052–1061. [CrossRef]
3. Wang, J.; Li, Y.; Liu, X.; Shen, C.; Zhang, H.; Xiong, K. Recent active thermal management technologies for the development of energy-optimized aerospace vehicles in China. *Chin. J. Aeronaut.* **2021**, *34*, 1–27. [CrossRef]
4. Abdullah, M.F.; Mat Hussin, M.R.; Ismail, M.A.; Wan Sabli, S.K. Chip-level thermal management in GaN HEMT: Critical review on recent patents and inventions. *Microelectron. Eng.* **2023**, *273*, 111958. [CrossRef]
5. El Kassar, R.; Al Takash, A.; Faraj, J.; Hammoud, M.; Khaled, M.; Ramadan, H.S. Recent advances in lithium-ion battery integration with thermal management systems for electric vehicles: A summary review. *J. Energy Storage* **2024**, *91*, 112061. [CrossRef]
6. Zhao, Y.; Dan, D.; Zheng, S.; Wei, M.; Xie, Y. A two-stage eco-cooling control strategy for electric vehicle thermal management system considering multi-source information fusion. *Energy* **2023**, *267*, 126606. [CrossRef]
7. Vikram, S.; Vashisht, S.; Rakshit, D.; Wan, M.P. Recent advancements and performance implications of hybrid battery thermal management systems for Electric Vehicles. *J. Energy Storage* **2024**, *90*, 111814. [CrossRef]
8. Vasiliev, L.; Lossouarn, D.; Romestant, C.; Alexandre, A.; Bertin, Y.; Piatsiushyk, Y.; Romanenkov, V. Loop heat pipe for cooling of high-power electronic components. *Int. J. Heat Mass Transf.* **2009**, *52*, 301–308. [CrossRef]
9. Putra, N.; Ariantara, B.; Pamungkas, R.A. Experimental investigation on performance of lithium-ion battery thermal management system using flat plate loop heat pipe for electric vehicle application. *Appl. Therm. Eng.* **2016**, *99*, 784–789. [CrossRef]
10. He, X.; Yan, W.; Wang, S. Study on heat transfer characteristics of a dual-evaporator ultra-thin loop heat pipe for laptop cooling. *Appl. Therm. Eng.* **2024**, *241*, 122395. [CrossRef]
11. Maydanik, Y.F. Loop heat pipes. *Appl. Therm. Eng.* **2005**, *25*, 635–657. [CrossRef]
12. Zhou, D.; Chen, Y.; Gao, W.; Xin, G. A novel thermal management scheme of 3D-IC based on loop heat pipe. *Int. J. Therm. Sci.* **2024**, *199*, 108906. [CrossRef]
13. Nakamura, K.; Ueno, A.; Nagano, H. Experimental study on long-distance anti-gravity loop heat pipe with submicron-scale porous structure. *Appl. Therm. Eng.* **2022**, *214*, 118793. [CrossRef]
14. Siedel, B.; Sartre, V.; Lefèvre, F. Literature review: Steady-state modelling of loop heat pipes. *Appl. Therm. Eng.* **2015**, *75*, 709–723. [CrossRef]
15. Wang, Z.; Yang, W. A review on loop heat pipe for use in solar water heating. *Energy Build.* **2014**, *79*, 143–154. [CrossRef]
16. Launay, S.; Sartre, V.; Bonjour, J. Analytical Model for Characterization of Loop Heat Pipes. *J. Thermophys. Heat Transf.* **2008**, *22*, 623–631. [CrossRef]
17. Qu, Y.; Wang, S.; Tian, Y. A review of thermal performance in multiple evaporators loop heat pipe. *Appl. Therm. Eng.* **2018**, *143*, 209–224. [CrossRef]
18. Launay, S.; Sartre, V.; Bonjour, J. Parametric analysis of loop heat pipe operation: A literature review. *Int. J. Therm. Sci.* **2007**, *46*, 621–636. [CrossRef]
19. Szymanski, P.; Mikielewicz, D.; Fooladpanjeh, S. Current Trends in Wick Structure Construction in Loop Heat Pipes Applications: A Review. *Materials* **2022**, *15*, 5765. [CrossRef]
20. Ahmed, S.; Pandey, M.; Kawaji, M. Loop Heat Pipe Design: An Evaluation of Recent Research on the Selection of Evaporator, Wick, and Working Fluid. *J. Therm. Sci. Eng. Appl.* **2022**, *14*, 070801. [CrossRef]
21. Mousa, M.M.; Abdel-Baky, M.A.; Eltantawy, I.M.; El-Sebaey, M.S. Proposing Novel Approach for Solar Still Performance Enhancement by Using Gravity Assisted Heat Pipes: Experimental and CFD Modeling. *ERJ. Eng. Res. J.* **2024**, *47*, 355–368. [CrossRef]
22. Mousa, M.M.; Abdel-Baky, M.A.; Eltantawy, I.M.; El-Sebaey, M.S. Experimental Investigation on the Effect of Inclination Angle of Flat Plate Solar Collector Using Gravity Assisted Heat Pipes. *ERJ. Eng. Res. J.* **2023**, *46*, 311–321. [CrossRef]
23. Riehl, R.R.; Mancin, S. Estimation of thermophysical properties for accurate numerical simulation of nanofluid heat transfer applied to a loop heat pipe. *Int. J. Thermofluids* **2022**, *14*, 100158. [CrossRef]
24. Ambirajan, A.; Adoni, A.A.; Vaidya, J.S.; Rajendran, A.A.; Kumar, D.; Dutta, P. Loop Heat Pipes: A Review of Fundamentals, Operation, and Design. *Heat Transf. Eng.* **2012**, *33*, 387–405. [CrossRef]

25. Huang, B.J.; Huang, H.H.; Liang, T.L. System dynamics model and startup behavior of loop heat pipe. *Appl. Therm. Eng.* **2009**, *29*, 2999–3005. [CrossRef]
26. Adachi, T.; Fujita, K.; Nagai, H. Numerical study of temperature oscillation in loop heat pipe. *Appl. Therm. Eng.* **2019**, *163*, 114281. [CrossRef]
27. He, J.; Miao, J.; Bai, L.; Lin, G.; Zhang, H.; Wen, D. Effect of non-condensable gas on the startup of a loop heat pipe. *Appl. Therm. Eng.* **2017**, *111*, 1507–1516. [CrossRef]
28. Dickey, J.T.; Peterson, G.P. Experimental and analytical investigation of a capillary pumped loop. *J. Thermophys. Heat Transf.* **1994**, *8*, 602–607. [CrossRef]
29. Kaya, T.; Hoang, T.T. Mathematical Modeling of Loop Heat Pipes and Experimental Validation. *J. Thermophys. Heat Transf.* **1999**, *13*, 314–320. [CrossRef]
30. Kaya, T.; Hoang, T.; Ku, J.; Cheung, M. Mathematical modeling of loop heat pipes. In Proceedings of the 37th Aerospace Sciences Meeting and Exhibit, Reno, NV, USA, 11–14 January 1999.
31. Hamdan, M.; Gerner, F.M.; Henderson, H.T. Steady state model of a loop heat pipe (LHP) with coherent porous silicon (CPS) wick in the evaporator. In Proceedings of the Ninteenth Annual IEEE Semiconductor Thermal Measurement and Management Symposium, San Jose, CA, USA, 11–13 March 2003; pp. 88–96.
32. Gabsi, I.; Maalej, S.; Zaghdoudi, M.C. Thermal performance modeling of loop heat pipes with flat evaporator for electronics cooling. *Microelectron. Reliab.* **2018**, *84*, 37–47. [CrossRef]
33. Bai, L.; Lin, G.; Zhang, H.; Wen, D. Mathematical modeling of steady-state operation of a loop heat pipe. *Appl. Therm. Eng.* **2009**, *29*, 2643–2654. [CrossRef]
34. Bai, L.; Lin, G.; Mu, Z.; Wen, D. Theoretical analysis of steady-state performance of a loop heat pipe with a novel evaporator. *Appl. Therm. Eng.* **2014**, *64*, 233–241. [CrossRef]
35. Bai, L.; Guo, J.; Lin, G.; He, J.; Wen, D. Steady-state modeling and analysis of a loop heat pipe under gravity-assisted operation. *Appl. Therm. Eng.* **2015**, *83*, 88–97. [CrossRef]
36. Jazebizadeh, H.; Kaya, T. Numerical and experimental investigation of the steady-state performance characteristics of loop heat pipes. *Appl. Therm. Eng.* **2020**, *181*, 115577. [CrossRef]
37. Qu, Y.; Qiao, S.; Zhou, D. Steady-state modelling of dual-evaporator loop heat pipe. *Appl. Therm. Eng.* **2021**, *193*, 116933. [CrossRef]
38. Fanxi, M.; Zhang, Q.; Du, S.; Yue, C.; Ma, X. One-dimensional steady-state mathematical model of a novel loop heat pipe with liquid line capillary wick. *Energy Explor. Exploit.* **2019**, *38*, 253–273. [CrossRef]
39. Du, S.; Zhang, Q.; Hou, P.; Yue, C.; Zou, S. Experimental study and steady-state model of a novel plate loop heat pipe without compensation chamber for CPU cooling. *Sustain. Cities Soc.* **2020**, *53*, 101894. [CrossRef]
40. Li, C.; Liu, Z.; Zhang, X. Steady-state operating characteristics analysis of loop heat pipes with flat-plate evaporator. *Therm. Sci. Eng. Prog.* **2022**, *28*, 101070. [CrossRef]
41. Xia, G.; Zhou, T.; Zhang, Y.; Jiao, G. Steady-state performance analysis of loop heat pipe radiator in space reactor. *Ann. Nucl. Energy* **2023**, *193*, 110053. [CrossRef]
42. Li, J.; Peterson, G.P. 3D heat transfer analysis in a loop heat pipe evaporator with a fully saturated wick. *Int. J. Heat Mass Transf.* **2011**, *54*, 564–574. [CrossRef]
43. Zhang, X.; Li, X.; Wang, S. Three-dimensional simulation on heat transfer in the flat evaporator of miniature loop heat pipe. *Int. J. Therm. Sci.* **2012**, *54*, 188–198. [CrossRef]
44. Chernysheva, M.A.; Maydanik, Y.F. Simulation of thermal processes in a flat evaporator of a copper–water loop heat pipe under uniform and concentrated heating. *Int. J. Heat Mass Transf.* **2012**, *55*, 7385–7397. [CrossRef]
45. Chernysheva, M.A.; Maydanik, Y.F. 3D-model for heat and mass transfer simulation in flat evaporator of copper-water loop heat pipe. *Appl. Therm. Eng.* **2012**, *33–34*, 124–134. [CrossRef]
46. Chernysheva, M.A.; Pastukhov, V.G.; Maydanik, Y.F. Analysis of heat exchange in the compensation chamber of a loop heat pipe. *Energy* **2013**, *55*, 253–262. [CrossRef]
47. Siedel, B.; Sartre, V.; Lefèvre, F. Complete analytical model of a loop heat pipe with a flat evaporator. *Int. J. Therm. Sci.* **2015**, *89*, 372–386. [CrossRef]
48. Muraoka, I.; Ramos, F.M.; Vlassov, V.V. Experimental and theoretical investigation of a capillary pumped loop with a porous element in the condenser. *Int. Commun. Heat Mass Transf.* **1998**, *25*, 1085–1094. [CrossRef]
49. Muraoka, I.; Ramos, F.M.; Vlassov, V.V. Analysis of the operational characteristics and limits of a loop heat pipe with porous element in the condenser. *Int. J. Heat Mass Transf.* **2001**, *44*, 2287–2297. [CrossRef]
50. Launay, S.; Platel, V.; Dutour, S.; Joly, J.-L. Transient Modeling of Loop Heat Pipes for the Oscillating Behavior Study. *J. Thermophys. Heat Transf.* **2007**, *21*, 487–495. [CrossRef]
51. Adachi, T.; Chang, X.; Nagai, H.; Takahashi, S. Numerical investigation on necessary condition for temperature oscillation in loop heat pipe. *Int. J. Therm. Sci.* **2024**, *196*, 108704. [CrossRef]
52. Ren, C.; Wu, Q.-S.; Hu, M.-B. Heat transfer with flow and evaporation in loop heat pipe's wick at low or moderate heat fluxes. *Int. J. Heat Mass Transf.* **2007**, *50*, 2296–2308. [CrossRef]
53. Shukla, K.N. Thermo-fluid dynamics of Loop Heat Pipe operation. *Int. Commun. Heat Mass Transf.* **2008**, *35*, 916–920. [CrossRef]

54. Kaya, T.; Pérez, R.; Gregori, C.; Torres, A. Numerical simulation of transient operation of loop heat pipes. *Appl. Therm. Eng.* **2008**, *28*, 967–974. [CrossRef]
55. Vlassov, V.V.; Riehl, R.R. Mathematical model of a loop heat pipe with cylindrical evaporator and integrated reservoir. *Appl. Therm. Eng.* **2008**, *28*, 942–954. [CrossRef]
56. Li, Y.Z.; Wang, Y.Y.; Lee, K.M. Dynamic Modeling and Transient Performance Analysis of a LHP-MEMS Thermal Management System for Spacecraft Electronics. *IEEE Trans. Compon. Packag. Technol.* **2010**, *33*, 597–606. [CrossRef]
57. Boubaker, R.; Platel, V. Dynamic model of capillary pumped loop with unsaturated porous wick for terrestrial application. *Energy* **2016**, *111*, 402–413. [CrossRef]
58. Bernagozzi, M.; Charmer, S.; Georgoulas, A.; Malavasi, I.; Michè, N.; Marengo, M. Lumped parameter network simulation of a Loop Heat Pipe for energy management systems in full electric vehicles. *Appl. Therm. Eng.* **2018**, *141*, 617–629. [CrossRef]
59. Zhang, Y.; Liu, J.; Liu, L.; Jiang, H.; Luan, T. Numerical simulation and analysis of heat leakage reduction in loop heat pipe with carbon fiber capillary wick. *Int. J. Therm. Sci.* **2019**, *146*, 106100. [CrossRef]
60. He, F.-L.; Du, W.-F.; Zhao, J.-F.; Li, J.-D.; Miao, J.-Y.; He, J. Numerical Simulation on the Effects of Component Layout Orientation on the Performance of a Neon-Charged Cryogenic Loop Heat Pipe. *Microgravity Sci. Technol.* **2020**, *32*, 179–188. [CrossRef]
61. Hashimoto, M.; Akizuki, Y.; Sato, K.; Ueno, A.; Nagano, H. Proposal, transient model, and experimental verification of loop heat pipe as heating device for electric-vehicle batteries. *Appl. Therm. Eng.* **2022**, *211*, 118432. [CrossRef]
62. Hoang, T.T.; Baldauff, R.W.; Mahony, D.R. Analytical Model for Transient Loop Heat Pipe Operation. In Proceedings of the 53rd AIAA Aerospace Sciences Meeting, Kissimmee, FL, USA, 5–9 January 2015.
63. Zhang, Z.; Cui, H.; Zhao, S.; Zhao, R.; Wu, T.; Liu, Z.; Liu, W. Simulation of heat and mass transfer process in a flat-plate loop heat pipe and experimental comparison. *Appl. Therm. Eng.* **2023**, *220*, 119705. [CrossRef]
64. Li, J.; Wang, D.; Peterson, G.P. Experimental studies on a high performance compact loop heat pipe with a square flat evaporator. *Appl. Therm. Eng.* **2010**, *30*, 741–752. [CrossRef]
65. Song, H.; Zhi-chun, L.; Jing, Z.; Chi, J.; Jin-guo, Y.; Wei, L. Experimental study of an ammonia loop heat pipe with a flat plate evaporator. *Int. J. Heat Mass Transf.* **2016**, *102*, 1050–1055. [CrossRef]
66. Wang, D.; Liu, Z.; Shen, J.; Jiang, C.; Chen, B.; Yang, J.; Tu, Z.; Liu, W. Experimental study of the loop heat pipe with a flat disk-shaped evaporator. *Exp. Therm. Fluid Sci.* **2014**, *57*, 157–164. [CrossRef]
67. Hong, S.; Wang, S.; Zhang, Z. Multiple orientations research on heat transfer performances of Ultra-Thin Loop Heat Pipes with different evaporator structures. *Int. J. Heat Mass Transf.* **2016**, *98*, 415–425. [CrossRef]
68. Zhou, G.; Li, J. Two-phase flow characteristics of a high performance loop heat pipe with flat evaporator under gravity. *Int. J. Heat Mass Transf.* **2018**, *117*, 1063–1074. [CrossRef]
69. Tian, W.; He, S.; Liu, Z.; Liu, W. Experimental investigation of a miniature loop heat pipe with eccentric evaporator for cooling electronics. *Appl. Therm. Eng.* **2019**, *159*, 113982. [CrossRef]
70. Odagiri, K.; Nagano, H. Heat transfer characteristics of flat evaporator loop heat pipe under high heat flux condition with different orientations. *Appl. Therm. Eng.* **2019**, *153*, 828–836. [CrossRef]
71. Maydanik, Y.F.; Vershinin, S.V.; Chernysheva, M.A. The results of comparative analysis and tests of ammonia loop heat pipes with cylindrical and flat evaporators. *Appl. Therm. Eng.* **2018**, *144*, 479–487. [CrossRef]
72. Wang, H.; Lin, G.; Shen, X.; Zhang, H. Three-Year Performance Test of a Dual Compensation Chamber Loop Heat Pipe. In Proceedings of the 2019 IEEE 10th International Conference on Mechanical and Aerospace Engineering (ICMAE), Brussels, Belgium, 22–25 July 2019; pp. 502–506.
73. Zhang, H.; Li, G.; Chen, L.; Man, G.; Miao, J.; Ren, X.; He, J.; Huo, Y. Development of Flat-Plate Loop Heat Pipes for Spacecraft Thermal Control. *Microgravity Sci. Technol.* **2019**, *31*, 435–443. [CrossRef]
74. Li, X.; Zhu, K.; Li, H.; Chen, X.; Wang, Y. Performance comparison regarding loop heat pipes with different evaporator structures. *Int. J. Therm. Sci.* **2019**, *136*, 86–95. [CrossRef]
75. Xiong, K.; Meng, L.; Wang, S. Design, fabrication, investigation and analysis of a novel flat evaporator loop heat pipe for cooling high heat flux server chips. *Appl. Therm. Eng.* **2022**, *201*, 117775. [CrossRef]
76. Ku, J. Heat Load Sharing in Loop Heat Pipes with Multiple Evaporators and Multiple Condensers. In Proceedings of the 9th AIAA/ASME Joint Thermophysics and Heat Transfer Conference, San Francisco, CA, USA, 5–8 June 2006.
77. Chang, X.; Watanabe, N.; Nagano, H. Visualization study of a loop heat pipe with two evaporators and one condenser under gravity-assisted condition. *Int. J. Heat Mass Transf.* **2019**, *135*, 378–391. [CrossRef]
78. Chang, X.; Watanabe, N.; Nagai, H.; Nagano, H. Visualization of thermo-fluid behavior of loop heat pipe with two evaporators and one condenser under various orientations with uneven heat loads. *Int. J. Heat Mass Transf.* **2024**, *221*, 125054. [CrossRef]
79. Qu, Y.; Zhou, D.; Qiao, S.; Zhou, K.; Tian, Y. Experimental study on the startup performance of dual-evaporator loop heat pipes. *Int. J. Therm. Sci.* **2021**, *170*, 107168. [CrossRef]
80. He, S.; Ma, Z.; Deng, W.; Zhang, Z.; Guo, Z.; Liu, W.; Liu, Z. Experimental investigation on the start-up performance of a novel flat loop heat pipe with dual evaporators. *Energy Rep.* **2022**, *8*, 7500–7507. [CrossRef]
81. Wu, T.; Wang, T.; Ma, Z.; Zhang, Z.; Liu, W.; Liu, Z. Experimental investigation on the start-up performance of a loop heat pipe with three flat disk evaporators combined. *Appl. Therm. Eng.* **2022**, *216*, 119128. [CrossRef]
82. Lu, D.; Xie, R.; Wen, J. Experimental Study on a Multi-Evaporator Loop Heat Pipe with a Dual-Layer Structure Condenser. *J. Therm. Sci.* **2023**, *32*, 1466–1476. [CrossRef]

83. Giraudon, R.; Lips, S.; Fabrègue, D.; Gremillard, L.; Maire, E.; Sartre, V. Effect of surface properties of capillary structures on the thermal behaviour of a LHP flat disk-shaped evaporator. *Int. J. Therm. Sci.* **2019**, *142*, 163–175. [CrossRef]
84. Yeh, C.-C.; Chen, C.-N.; Chen, Y.-M. Heat transfer analysis of a loop heat pipe with biporous wicks. *Int. J. Heat Mass Transf.* **2009**, *52*, 4426–4434. [CrossRef]
85. Zhang, Z.; Zhao, R.; Liu, Z.; Liu, W. Application of biporous wick in flat-plate loop heat pipe with long heat transfer distance. *Appl. Therm. Eng.* **2021**, *184*, 116283. [CrossRef]
86. Ji, X.; Wang, Y.; Xu, J.; Huang, Y. Experimental study of heat transfer and start-up of loop heat pipe with multiscale porous wicks. *Appl. Therm. Eng.* **2017**, *117*, 782–798. [CrossRef]
87. Ling, W.; Zhou, W.; Liu, R.; Qiu, Q.; Liu, J. Thermal performance of loop heat pipe with porous copper fiber sintered sheet as wick structure. *Appl. Therm. Eng.* **2016**, *108*, 251–260. [CrossRef]
88. Ling, W.; Zhou, W.; Liu, R.; Qiu, Q.; Ke, Y. Operational characteristics of loop heat pipes with porous copper fiber sintered sheet as wick. *Appl. Therm. Eng.* **2017**, *122*, 398–408. [CrossRef]
89. Hu, Z.; Wang, D.; Xu, J.; Zhang, L. Development of a loop heat pipe with the 3D printed stainless steel wick in the application of thermal management. *Int. J. Heat Mass Transf.* **2020**, *161*, 120258. [CrossRef]
90. Zhang, S.; Lin, L.; Chen, G.; Tang, H.; Zeng, J.; Yuan, W.; Tang, Y. Experimental study on the capillary performance of aluminum micro-grooved wicks with reentrant cavity array. *Int. J. Heat Mass Transf.* **2019**, *139*, 917–927. [CrossRef]
91. Deng, D.; Liang, D.; Tang, Y.; Peng, J.; Han, X.; Pan, M. Evaluation of capillary performance of sintered porous wicks for loop heat pipe. *Exp. Therm. Fluid Sci.* **2013**, *50*, 1–9. [CrossRef]
92. Corrochano, J.; Prado-Montes, P.; Torres, A. Thermophysical and Mechanical Characterization of Nickel and Stainless Steel Sintered Wicks. *J. Porous Media* **2019**, *22*, 713–722. [CrossRef]
93. Esarte, J.; Blanco, J.M.; Bernardini, A.; Sancibrián, R. Performance Assessment of a Three-Dimensional Printed Porous Media Produced by Selective Laser Melting Technology for the Optimization of Loop Heat Pipe Wicks. *Appl. Sci.* **2019**, *9*, 2905. [CrossRef]
94. Wu, S.-C.; Gu, T.-W.; Wang, D.; Chen, Y.-M. Study of PTFE wick structure applied to loop heat pipe. *Appl. Therm. Eng.* **2015**, *81*, 51–57. [CrossRef]
95. Wu, S.-C.; Lin, Z.-H.; Lo, S.; Lin, W.-J. Effect of PTFE wick thickness on Loop heat pipe performance. *Therm. Sci. Eng. Prog.* **2023**, *42*, 101911. [CrossRef]
96. Wu, S.-C.; Lee, T.-J.; Lin, W.-J.; Chen, Y.-M. Study of self-rewetting fluid applied to loop heat pipe with PTFE wick. *Appl. Therm. Eng.* **2017**, *119*, 622–628. [CrossRef]
97. Nishikawara, M.; Nagano, H. Parametric experiments on a miniature loop heat pipe with PTFE wicks. *Int. J. Therm. Sci.* **2014**, *85*, 29–39. [CrossRef]
98. He, S.; Zhou, P.; Ma, Z.; Deng, W.; Zhang, H.; Chi, Z.; Liu, W.; Liu, Z. Experimental study on transient performance of the loop heat pipe with a pouring porous wick. *Appl. Therm. Eng.* **2020**, *164*, 114450. [CrossRef]
99. Xu, J.; Wang, D.; Hu, Z.; Zhang, L.; Ye, L.; Zhou, Y. Effect of the working fluid transportation in the copper composite wick on the evaporation efficiency of a flat loop heat pipe. *Appl. Therm. Eng.* **2020**, *178*, 115515. [CrossRef]
100. Wang, D.; Wang, J.; Bao, X.; Chen, G.; Chu, H. Experimental study on hydraulic and thermal characteristics of composite porous wick with spherical–dendritic powders. *J. Therm. Anal. Calorim.* **2020**, *141*, 107–117. [CrossRef]
101. Yang, P.; Yang, T.; Gao, T.; Zhao, S.; Liu, J.; Zhang, P. Experimental study on a dual compensation chamber loop heat pipe with a ceramic wick. *Appl. Therm. Eng.* **2023**, *230*, 120750. [CrossRef]
102. Zhou, W.; Ling, W.; Duan, L.; Hui, K.S.; Hui, K.N. Development and tests of loop heat pipe with multi-layer metal foams as wick structure. *Appl. Therm. Eng.* **2016**, *94*, 324–330. [CrossRef]
103. Silk, E.A.; Myre, D. Fractal Loop Heat Pipe performance testing with a compressed carbon foam wick structure. *Appl. Therm. Eng.* **2013**, *59*, 290–297. [CrossRef]
104. Liu, J.; Zhang, Y.; Feng, C.; Liu, L.; Luan, T. Study of copper chemical-plating modified polyacrylonitrile-based carbon fiber wick applied to compact loop heat pipe. *Exp. Therm. Fluid Sci.* **2019**, *100*, 104–113. [CrossRef]
105. Guo, H.; Ji, X.; Xu, J. Enhancement of loop heat pipe heat transfer performance with superhydrophilic porous wick. *Int. J. Therm. Sci.* **2020**, *156*, 106466. [CrossRef]
106. Guo, H.; Ji, X.; Gan, Y.; Xu, J. Experimental study on the heat transfer performance of loop heat pipe with different particle morphology and wettability of porous wick. *Int. J. Therm. Sci.* **2023**, *186*, 108134. [CrossRef]
107. Solomon, A.B.; Mahto, A.K.; Joy, R.C.; Rajan, A.A.; Jayprakash, D.A.; Dixit, A.; Sahay, A. Application of bio-wick in compact loop heat pipe. *Appl. Therm. Eng.* **2020**, *169*, 114927. [CrossRef]
108. Gregori, C.; Mishkinis, D.; Prado, P.; Torres, A.; Pérez, R. *Loop Heat Pipe Technology for Aircraft Anti-Icing Applications*; SAE Technical Paper 0148-7191; SAE International: Warrendale, PA, USA, 2007.
109. Faghri, A. *Heat Pipe Science and Technology*; Global Digital Press: Jaipur, India, 1995.
110. Anand, A.; Jaiswal, A.; Ambirajan, A.; Dutta, P. Performance assessment of loop heat pipe using modified figure of merit with correction factor. In Proceedings of the 24th National and 2nd International ISHMT-ASTFE Heat and Mass Transfer Conference (IHMTC-2017), Hyderabad, India, 27–30 December 2017.
111. Singh, R.; Nguyen, T.; Mochizuki, M.; Akbarzadeh, A. Working fluid study for loop heat pipes. *Therm. Sci. Eng. Prog.* **2022**, *35*, 101451. [CrossRef]

112. Liu, C.; Xie, R.; Li, N.; Lu, D.; Hong, F.; Wu, Y. Experimental study of loop heat pipes with different working fluids in 190–260 K. *Appl. Therm. Eng.* **2020**, *178*, 115530. [CrossRef]
113. Xu, G.; Xie, R.; Li, N.; Liu, C. Experimental Investigation of a Loop Heat Pipe With R245fa and R1234ze(E) as Working Fluids. *J. Therm. Sci. Eng. Appl.* **2021**, *14*, 041014. [CrossRef]
114. Szymański, P.; Mikielewicz, D. Challenges in operating and testing loop heat pipes in 500–700 K temperature ranges. *Arch. Thermodyn.* **2022**, *43*, 61–73. [CrossRef]
115. Gakal, P.; Mishkinis, D.; Leilands, A.; Usakovs, I.; Orlov, R.; Rogoviy, Y. Analysis of working fluids applicable for high-temperature loop heat pipe applications. *IOP Conf. Ser. Mater. Sci. Eng.* **2022**, *1226*, 012036. [CrossRef]
116. Zini, A.; Socci, L.; Vaccaro, G.; Rocchetti, A.; Talluri, L. Working Fluid Selection for High-Temperature Heat Pumps: A Comprehensive Evaluation. *Energies* **2024**, *17*, 1556. [CrossRef]
117. Durán-Sánchez, A.; Álvarez-García, J.; Del Río-Rama, M.D. Sustainable Water Resources Management: A Bibliometric Overview. *Water* **2018**, *10*, 1191. [CrossRef]
118. Zhang, D.; Yang, M.; Feng, X. Aromatics production from methanol and pentane: Conceptual process design, comparative energy and techno-economic analysis. *Comput. Chem. Eng.* **2019**, *126*, 178–188. [CrossRef]
119. Yang, J.; Ye, Z.; Yu, B.; Ouyang, H.; Chen, J. Simultaneous experimental comparison of low-GWP refrigerants as drop-in replacements to R245fa for Organic Rankine cycle application: R1234ze(Z), R1233zd(E), and R1336mzz(E). *Energy* **2019**, *173*, 721–731. [CrossRef]
120. Qyyum, M.A.; Khan, A.; Ali, S.; Khurram, M.S.; Mao, N.; Naquash, A.; Noon, A.A.; He, T.; Lee, M. Assessment of working fluids, thermal resources and cooling utilities for Organic Rankine Cycles: State-of-the-art comparison, challenges, commercial status, and future prospects. *Energy Convers. Manag.* **2022**, *252*, 115055. [CrossRef]
121. Jafarinejad, S. *Petroleum Waste Treatment and Pollution Control*; Butterworth-Heinemann: Oxford, UK, 2016.
122. Maydanik, Y.; Chernysheva, M.; Vershinin, S. High-Capacity Loop Heat Pipe with Flat Evaporator for Efficient Cooling Systems. *J. Thermophys. Heat Transf.* **2020**, *34*, 465–475. [CrossRef]
123. Anand, A.R.; Jaiswal, A.; Ambirajan, A.; Dutta, P. Experimental studies on a miniature loop heat pipe with flat evaporator with various working fluids. *Appl. Therm. Eng.* **2018**, *144*, 495–503. [CrossRef]
124. Zhang, H.; Jiang, C.; Zhang, Z.; Liu, Z.; Luo, X.; Liu, W. A study on thermal performance of a pump-assisted loop heat pipe with ammonia as working fluid. *Appl. Therm. Eng.* **2020**, *175*, 115342. [CrossRef]
125. Jasvanth, V.S.; Adoni, A.A.; Jaikumar, V.; Ambirajan, A. Design and testing of an ammonia loop heat pipe. *Appl. Therm. Eng.* **2017**, *111*, 1655–1663. [CrossRef]
126. Zhao, R.; Zhang, Z.; Zhao, S.; Cui, H.; Liu, Z.; Liu, W. Experimental study of flat-disk loop heat pipe with R1233zd(E) for cooling terrestrial electronics. *Appl. Therm. Eng.* **2021**, *197*, 117385. [CrossRef]
127. Wang, H.; Lin, G.; Bai, L.; Tao, Y.; Wen, D. Comparative study of two loop heat pipes using R134a as the working fluid. *Appl. Therm. Eng.* **2020**, *164*, 114459. [CrossRef]
128. Xiong, C.; Bai, L.; Li, H.; Guo, Y.; Yu, Y.; Lin, G. Experimental study on a R134a loop heat pipe with high heat transfer capacity. *Heat Mass Transf.* **2022**, *58*, 903–916. [CrossRef]
129. Senthilkumar, C.; Krishnan, A.S.; Solomon, A.B. Effect of thin porous copper coating on the performance of wickless heat pipe with R134a as working fluid. *J. Therm. Anal. Calorim.* **2020**, *139*, 963–973. [CrossRef]
130. Jose, J.; Baby, R. Enhancement of the thermal performance of a loop heat pipe using silica-water nanofluid. *J. Phys. Conf. Ser.* **2019**, *1355*, 012010. [CrossRef]
131. Stephen, E.N.; Asirvatham, L.G.; Kandasamy, R.; Solomon, B.; Kondru, G.S. Heat transfer performance of a compact loop heat pipe with alumina and silver nanofluid. *J. Therm. Anal. Calorim.* **2019**, *136*, 211–222. [CrossRef]
132. Zhao, T.; Ma, Z.; Zhang, Z.; Deng, W.; Long, R.; Liu, W.; Ma, L.; Liu, Z. Experimental investigation of a loop heat pipe with a flat evaporator and cupric oxide nanofluids as working fluid. *Energy Rep.* **2021**, *7*, 7693–7703. [CrossRef]
133. Wan, Z.; Deng, J.; Li, B.; Xu, Y.; Wang, X.; Tang, Y. Thermal performance of a miniature loop heat pipe using water–copper nanofluid. *Appl. Therm. Eng.* **2015**, *78*, 712–719. [CrossRef]
134. Harun, M.A.B.; Gunnasegaran, P.A.L.; Sidik, N.A.C.; Beriache, M.h.; Ghaderian, J. Experimental investigation and optimization of loop heat pipe performance with nanofluids. *J. Therm. Anal. Calorim.* **2021**, *144*, 1435–1449. [CrossRef]
135. Aun, T.S.; Abdullah, M.Z.; Gunnasegaran, P. Influence of low concentration of diamond water nanofluid in loop heat pipe. *Int. J. Heat Technol.* **2017**, *35*, 539–548. [CrossRef]
136. Gunnasegaran, P.; Abdullah, M.Z.; Shuaib, N.H. Influence of nanofluid on heat transfer in a loop heat pipe. *Int. Commun. Heat Mass Transf.* **2013**, *47*, 82–91. [CrossRef]
137. Gunnasegaran, P.; Abdullah, M.Z.; Yusoff, M.Z.; Kanna, R. Heat Transfer in a Loop Heat Pipe using Diamond-H_2O Nanofluid. *Heat Transf. Eng.* **2018**, *39*, 1117–1131. [CrossRef]
138. Tharayil, T.; Asirvatham, L.G.; Ravindran, V.; Wongwises, S. Thermal performance of miniature loop heat pipe with graphene–water nanofluid. *Int. J. Heat Mass Transf.* **2016**, *93*, 957–968. [CrossRef]
139. Adoni, A.A.; Ambirajan, A.; Jasvanth, V.; Kumar, D.; Dutta, P. Effects of mass of charge on loop heat pipe operational characteristics. *J. Thermophys. Heat Transf.* **2009**, *23*, 346–355. [CrossRef]
140. Mo, Q.; Liang, J. Operational performance of a cryogenic loop heat pipe with insufficient working fluid inventory. *Int. J. Refrig.* **2006**, *29*, 519–527. [CrossRef]

141. Nagano, H.; Onogawa, E.; Fukuyoshi, F.; Ogawa, H.; Nagai, H. Effect of amount of fluid charge in thermal performance of loop heat pipe. *Heat Transf.—Asian Res.* **2010**, *39*, 355–364. [CrossRef]
142. Wang, S.; Huo, J.; Zhang, X.; Lin, Z. Experimental study on operating parameters of miniature loop heat pipe with flat evaporator. *Appl. Therm. Eng.* **2012**, *40*, 318–325. [CrossRef]
143. Zhang, L.; Xu, J.; Xu, H. Effect of inventory on the heat performance of copper–water loop heat pipe. *Exp. Therm. Fluid Sci.* **2013**, *44*, 875–882. [CrossRef]
144. Smitka, M.; Kolková, Z.; Nemec, P.; Malcho, M. Impact of the amount of working fluid in loop heat pipe to remove waste heat from electronic component. *EPJ Web Conf.* **2014**, *67*, 02109. [CrossRef]
145. Blauciak, K.; Szymanski, P.; Mikielewicz, D. The Influence of Loop Heat Pipe Evaporator Porous Structure Parameters and Charge on Its Effectiveness for Ethanol and Water as Working Fluids. *Materials* **2021**, *14*, 7029. [CrossRef] [PubMed]
146. d'Entremont, B.; Ochterbeck, J. Charging considerations effects in ground testing loop heat pipes. In Proceedings of the 49th International Conference on Environmental Systems, Boston, MA, USA, 7–11 July 2019.
147. Song, W.; Xu, Y.; Xue, L.; Li, H.; Guo, C. Visualization Experimental Study on Silicon-Based Ultra-Thin Loop Heat Pipe Using Deionized Water as Working Fluid. *Micromachines* **2021**, *12*, 1080. [CrossRef]
148. Hongxing, Z.; Guiping, L.; Ting, D.; Wei, Y.; Xingguo, S.; Sudakov, R.G.; Maidanik, Y.F. Investigation On Startup Behaviors of a Loop Heat Pipe. *J. Thermophys. Heat Transf.* **2005**, *19*, 509–518. [CrossRef]
149. Rodriguez, J.I.; Pauken, M.; Na-Nakornpanom, A. *Transient Characterization of a Propylene Loop Heat Pipe during Startup and Shut-Down*; SAE Technical Paper 0148-7191; SAE International: Warrendale, PA, USA, 2000.
150. Lu, X.-Y.; Hua, T.-C.; Liu, M.-J.; Cheng, Y.-X. Thermal analysis of loop heat pipe used for high-power LED. *Thermochim. Acta* **2009**, *493*, 25–29. [CrossRef]
151. Bai, L.; Lin, G.; Wen, D.; Feng, J. Experimental investigation of startup behaviors of a dual compensation chamber loop heat pipe with insufficient fluid inventory. *Appl. Therm. Eng.* **2009**, *29*, 1447–1456. [CrossRef]
152. Bai, L.; Tao, Y.; Guo, Y.; Lin, G. Startup characteristics of a dual compensation chamber loop heat pipe with an extended bayonet tube. *Int. J. Heat Mass Transf.* **2020**, *148*, 119066. [CrossRef]
153. Chernysheva, M.A.; Maydanik, Y.F.; Ochterbeck, J.M. Heat Transfer Investigation in Evaporator of Loop Heat Pipe During Startup. *J. Thermophys. Heat Transf.* **2008**, *22*, 617–622. [CrossRef]
154. Wang, S.; Zhang, W.; Zhang, X.; Chen, J. Study on start-up characteristics of loop heat pipe under low-power. *Int. J. Heat Mass Transf.* **2011**, *54*, 1002–1007. [CrossRef]
155. Bai, L.; Yang, Z.; Shen, X.; Guo, Y.; Lin, G.; Wen, D. Startup characteristics of an ammonia loop heat pipe with a rectangular evaporator. *Heat Mass Transf.* **2022**, *58*, 813–831. [CrossRef]
156. Hoang, T.; Baldauff, R.; Cheung, K. Start-Up Behavior of an Ammonia Loop Heat Pipe. In Proceedings of the 3rd International Energy Conversion Engineering Conference, San Francisco, CA, USA, 15–18 August 2005.
157. Boo, J.H.; Jung, E.G. Bypass line assisted start-up of a loop heat pipe with a flat evaporator. *J. Mech. Sci. Technol.* **2009**, *23*, 1613–1619. [CrossRef]
158. Wang, L.; Miao, J.; Gong, M.; Zhou, Q.; Liu, C.; Zhang, H.; Fan, H. Research on the Heat Transfer Characteristics of a Loop Heat Pipe Used as Mainline Heat Transfer Mode for Spacecraft. *J. Therm. Sci.* **2019**, *28*, 736–744. [CrossRef]
159. Wang, X.; Wei, J. Visual investigation on startup characteristics of a novel loop heat pipe. *Appl. Therm. Eng.* **2016**, *105*, 198–208. [CrossRef]
160. Nishikawara, M.; Otani, K.; Ueda, Y.; Yanada, H. Liquid–vapor phase behavior and operating characteristics of the capillary evaporator of a loop heat pipe at start-up. *Int. J. Therm. Sci.* **2018**, *129*, 426–433. [CrossRef]
161. Ku, J.; Rodriguez, J.I. *Low Frequency High Amplitude Temperature Oscillations in Loop Heat Pipe Operation*; SAE Technical Paper 0148-7191; SAE International: Warrendale, PA, USA, 2003.
162. Singh, R.; Akbarzadeh, A.; Mochizuki, M. Operational characteristics of a miniature loop heat pipe with flat evaporator. *Int. J. Therm. Sci.* **2008**, *47*, 1504–1515. [CrossRef]
163. Celata, G.P.; Cumo, M.; Furrer, M. Experimental tests of a stainless steel loop heat pipe with flat evaporator. *Exp. Therm. Fluid Sci.* **2010**, *34*, 866–878. [CrossRef]
164. Zhang, X.; Huo, J.; Wang, S. Experimental investigation on temperature oscillation in a miniature loop heat pipe with flat evaporator. *Exp. Therm. Fluid Sci.* **2012**, *37*, 29–36. [CrossRef]
165. Liu, Z.; Li, H.; Chen, B.; Yang, J.; Liu, W. Operational characteristics of flat type loop heat pipe with biporous wick. *Int. J. Therm. Sci.* **2012**, *58*, 180–185. [CrossRef]
166. Hoang, T.; Baldauff, R. A Theory for Temperature Oscillations in Loop Heat Pipes. In Proceedings of the 42nd International Conference on Environmental Systems, San Francisco, CA, USA, 15–19 July 2012.
167. Feng, J.; Lin, G.; Bai, L. Experimental investigation on operating instability of a dual compensation chamber loop heat pipe. *Sci. China Ser. E Technol. Sci.* **2009**, *52*, 2316–2322. [CrossRef]
168. Lv, X.; Xie, Y.; Zhang, H.; Xu, Y.; Wu, H.; Day, R.; Ren, J. Temperature oscillation of a dual compensation chamber loop heat pipe under acceleration conditions. *Appl. Therm. Eng.* **2021**, *198*, 117450. [CrossRef]
169. Yerkes, K.L.; Scofield, J.D.; Courson, D.L.; Jiang, H. Steady-Periodic Acceleration Effects on the Performance of a Loop Heat Pipe. *J. Thermophys. Heat Transf.* **2014**, *28*, 440–454. [CrossRef]

170. Mo, D.; Zou, G.; Lu, S.; Zhang, L.W. A Flow Visualization Study on the Temperature Oscillations Inside a Loop Heat Pipe With Flat Evaporator. In Proceedings of the ASME 2013 International Technical Conference and Exhibition on Packaging and Integration of Electronic and Photonic Microsystems, Burlingame, CA, USA, 16–18 July 2013.
171. Zhang, Q.; Lin, G.; Shen, X.; Bai, L.; Wen, D. Visualization study on the heat and mass transfer in the evaporator-compensation chamber of a loop heat pipe. *Appl. Therm. Eng.* **2020**, *164*, 114472. [CrossRef]
172. Liu, L.; Yang, X.; Yuan, B.; Wei, J. Investigation of temperature oscillations in a novel loop heat pipe with a vapor-driven jet injector. *Int. J. Heat Mass Transf.* **2021**, *179*, 121672. [CrossRef]
173. Li, X.; Zhang, Z.; Wang, Y.; Zhu, K.; Liu, S. Characteristic of temperature oscillation during the operation of loop heat pipe enhanced by pressure head of evaporation. *Heat Mass Transf.* **2022**, *58*, 1145–1155. [CrossRef]
174. Du, S.; Zhang, Q.; Ling, L.; Zou, S.; Liu, L.; Meng, F. Visualization Investigation on Temperature Oscillation and Two-Phase Behaviors of A Flat Loop Heat Pipe. *J. Therm. Sci.* **2023**, *32*, 1536–1546. [CrossRef]
175. Chen, B.B.; Liu, W.; Liu, Z.C.; Li, H.; Yang, J.G. Experimental investigation of loop heat pipe with flat evaporator using biporous wick. *Appl. Therm. Eng.* **2012**, *42*, 34–40. [CrossRef]
176. Liu, Z.; Wang, D.; Jiang, C.; Yang, J.; Liu, W. Experimental study on loop heat pipe with two-wick flat evaporator. *Int. J. Therm. Sci.* **2015**, *94*, 9–17. [CrossRef]
177. Mo, D.-C.; Ding, N.; Lu, S.-S. Gravity Effects on the Performance of a Flat Loop Heat Pipe. *Microgravity Sci. Technol.* **2009**, *21*, 95–102. [CrossRef]
178. Zakar, D.; Holman, T.D.; Maxwell, J.R.; Hoang, T.T.; Baldauff, R.W. Experimental Investigation of Temperature Oscillations in Loop Heat Pipes. In Proceedings of the 2018 AIAA Aerospace Sciences Meeting, Kissimmee, FL, USA, 8–12 January 2018.
179. Xu, J.; Wang, Z.; Xu, H.; Zhang, L. Experimental research on the heat performance of a flat copper-water loop heat pipe with different inventories. *Exp. Therm. Fluid Sci.* **2017**, *84*, 110–119. [CrossRef]
180. Hsu, C.-C.; Kang, S.-W.; Hou, T.-F. Performance Testing of Micro Loop Heat Pipes. *J. Appl. Sci. Eng.* **2005**, *8*, 123–132. [CrossRef]
181. Singh, R.; Akbarzadeh, A.; Mochizuki, M. Operational characteristics of the miniature loop heat pipe with non-condensable gases. *Int. J. Heat Mass Transf.* **2010**, *53*, 3471–3482. [CrossRef]
182. Prado-Montes, P.; Mishkinis, D.; Kulakov, A.; Torres, A.; Pérez-Grande, I. Effects of non condensable gas in an ammonia loop heat pipe operating up to 125 °C. *Appl. Therm. Eng.* **2014**, *66*, 474–484. [CrossRef]
183. Maydanik, Y.F.; Chernysheva, M.A.; Pastukhov, V.G. Investigation of thermal characteristics of high-capacity loop heat pipes after a long-term storage. *Energy* **2014**, *74*, 804–809. [CrossRef]
184. He, J.; Lin, G.; Bai, L.; Miao, J.; Zhang, H. Effect of non-condensable gas on the operation of a loop heat pipe. *Int. J. Heat Mass Transf.* **2014**, *70*, 449–462. [CrossRef]
185. Anand, A.R. Investigations on effect of noncondensable gas in a loop heat pipe with flat evaporator on deprime. *Int. J. Heat Mass Transf.* **2019**, *143*, 118531. [CrossRef]
186. Wang, H.; Lin, G.; Shen, X.; Bai, L.; Yang, R.; Sun, B. Effect of evaporator tilt on the startup performance of loop heat pipe with non-condensable gas. In Proceedings of the CSAA/IET International Conference on Aircraft Utility Systems (AUS 2018), Guiyang, China, 19–22 June 2018.
187. Wang, H.; Lin, G.; Shen, X.; Bai, L.; Wen, D. Effect of evaporator tilt on a loop heat pipe with non-condensable gas. *Int. J. Heat Mass Transf.* **2019**, *128*, 1072–1080. [CrossRef]
188. Wang, H.; Lin, G.; Shen, X.; Bai, L.; Yang, R.; Wen, D. Effect of evaporator/condenser elevations on a loop heat pipe with non-condensable gas. *Appl. Therm. Eng.* **2020**, *180*, 115711. [CrossRef]
189. Hartenstine, J.R.; Anderson, W.G.; Bonner, R., III. Titanium Loop Heat Pipes for Space Nuclear Power Systems. *AIP Conf. Proc.* **2008**, *969*, 44–52. [CrossRef]
190. Yang, R.; Lin, G.; He, J.; Bai, L.; Miao, J. Investigation on the effect of thermoelectric cooler on LHP operation with non-condensable gas. *Appl. Therm. Eng.* **2017**, *110*, 1189–1199. [CrossRef]